CHAPTER FIVE

EIS Study on the Solid Polymer Electrolytes (SPEs)

5.1 Introduction

The main aim of this chapter is to study the electrical and dielectric properties of CS:AgTf, CS:NaTf and CS:LiTf solid polymer electrolytes. The basic principle between DC conductivity and dielectric constant for these low salt concentration systems are presented. The bulk DC conductivity and bulk dielectric constant are calculated from the high frequency semicircle. The compensated Arrhenius behavior is also compared to the normal Arrhenius relation and the pre-exponential factor (σ_o) was studied as a function of temperature and dielectric constant. Furthermore the relaxations of ions were studied in terms of loss tangent and electric modulus. The correlation between impedance plots (Z_i-Z_r) and AC conductivity spectra were demonstrated. The ion conduction model for these chitosan based solid polymer electrolytes were specified from the temperature variation of the frequency exponent (s).

5.2 Electrical/Dielectric properties of SPEs based on CS:AgTf

5.2.1 DC conductivity and Dielectric analysis of SPE based on CS:AgTf

The room temperature conductivity of chitosan-$AgCF_3SO_3$ electrolyte with various salt contents is shown in Figure 5.1. It can be noted that the ionic conductivity of the chitosan based electrolyte increases with increasing $AgCF_3SO_3$ concentration up to 10 wt.% $AgCF_3SO_3$. The conductivity value at room temperature has been found to increase by more than two orders of magnitude from 1.73×10^{-10} S cm^{-1} for pure chitosan film to 4.25×10^{-8} S cm^{-1} for CSA6 sample. The increase in conductivity is attributable to the increase in number density of mobile ions ($\sigma = \Sigma qn\mu$) provided by the salt at room temperature. It can be seen (Fig.1) that there is competition between ion dissociation and association. At 4 wt.%, to 6 wt.%, the concentration of mobile ions remains almost equal resulting in conductivity to be approximately equal.

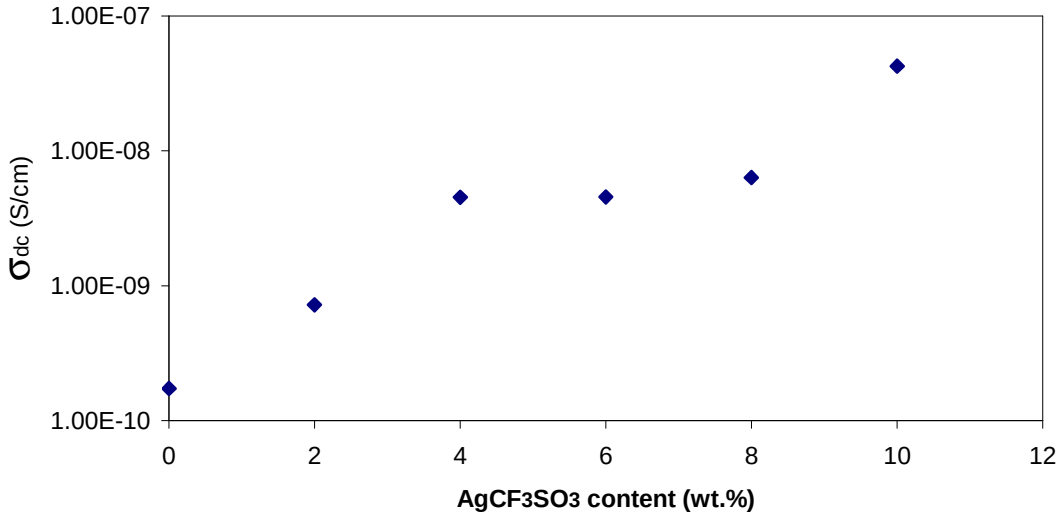

Figure 5.1 The ionic conductivity of chitosan with various $AgCF_3SO_3$ concentration.

Figure 5.2 shows the variation of DC conductivity of chitosan electrolyte as a function of temperature (log σ_{dc} versus $10^3/T$) for different concentrations of silver triflate.

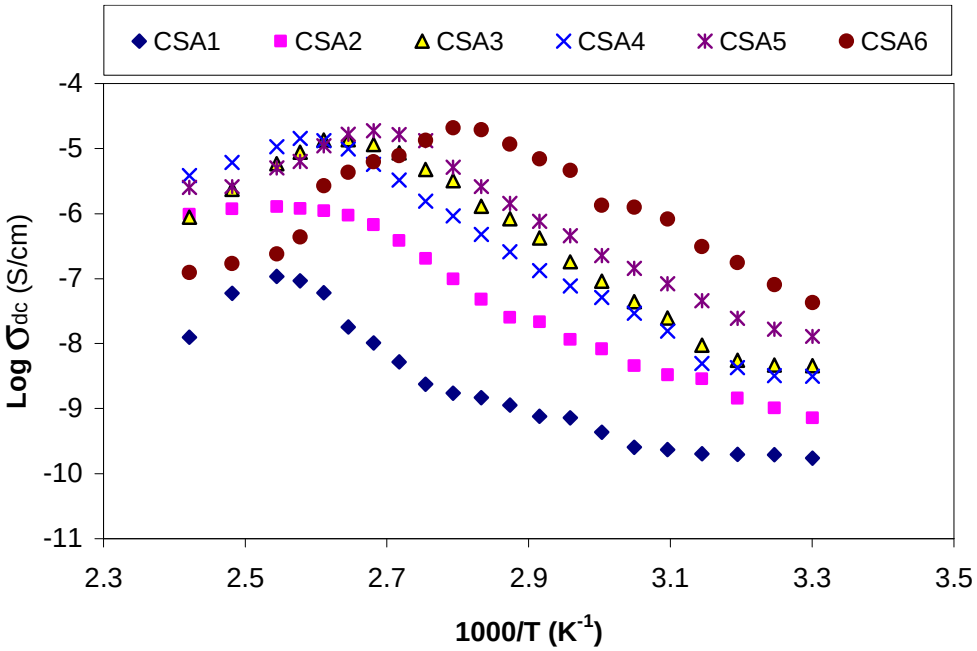

Figure 5.2 Temperature dependence of ionic conductivity of chitosan-silver triflate SPEs.

Conductivity increases with temperature up to a certain temperature after which the conductivity dropped. The temperature at which the conductivity begins to drop does not seem to follow any particular trend.

It is also noted that in the region where conductivity increases with temperature, there is no abrupt change in the value of conductivity with temperature. Yahya et al., (2006) reported that the non-existence of any abrupt jump indicates the fact that the chitosan-based electrolyte is completely amorphous. This is well supported by the X-ray diffractogram

where no distinct crystallite peak is observed for the sample CSA6. The linear increase in conductivity of the chitosan electrolyte with temperature before drop in conductivity occurs can be described by the Arrhenius equation,

$$\sigma = \sigma_o \exp^{(-E_a / K_B T)} \qquad (3.1)$$

where σ is the conductivity at temperature T (in Kelvin), K_B is the Boltzmann constant, E_a is the activation energy and σ_o is the pre-exponential factor. The activation energy, E_a may be deduced from the slope of log σ versus 1000/T plot. The calculated activation energy E_a for the highest conducting sample i.e., CA6 is 1.13 eV with the regression value R^2=0.99 in the temperature range between 303 K and 358 K. The electrical conductivity of chitosan-silver triflate membrane decreases at temperatures greater than 358 K (for CSA6). The drop in conductivity can be attributed to the reduction of silver ions to silver particles. Transformation from silver ions (Ag^+) to silver particles (Ag^o) reduce the number of silver ions that participate in conduction of charge as may be deduced from this equation ($\sigma = \Sigma qn\mu$). The presence of these silver particles creates grain boundaries that increase the resistance within the bulk of the material. The UV-vis and XRD results at different temperatures reveal the presence of silver nanoparticles and their growth as explained in previous chapter and completely supports the conductivity temperature relationships.

Fig. 5.3 shows the variation of dielectric constant as a function of frequency for different salt concentrations at 303 K. One of the main advantages of frequency dependent

measurements is that the contributions of the electrode polarization (low frequency, region I) and bulk materials (high frequency, region II) can be easily represented [Bassiouni et al., 2003]. It can be seen from Fig. 5.3, that ε' increases with increasing salt concentration from 2 to 4 wt.% and then decreases at 6 wt.%, which can be attributed to ion association. After that ε' continue to increase until 10 wt.% silver triflate.

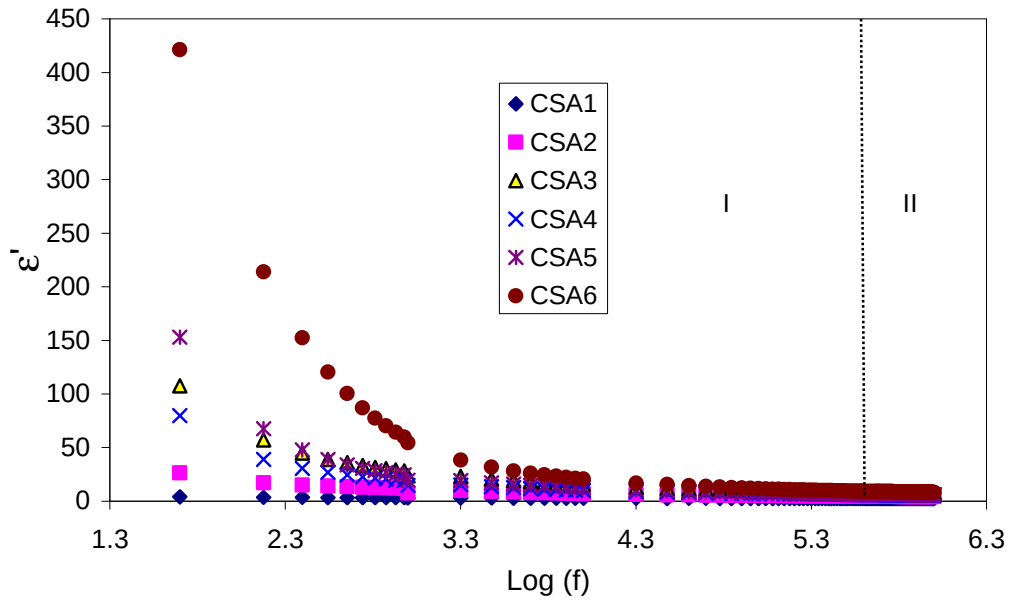

Figure 5.3. Composition dependence of dielectric constant for chitosan-silver triflate SPEs at 303 K.

Due to the high value of electrode polarization (EP), the bulk property of the materials which is represented at high frequencies is suppressed. However, the plot of the dielectric constant versus frequency for the bulk material at different salt concentrations can show the effect of salt concentration as depicted in Fig.5.4. The increase of ε' can be ascribed to the increase in the amount of charge stored in the sample i.e., the increase in the dielectric constant represents a fractional increase in charges stored within the chitosan-based electrolyte. The dependence of charge carrier concentration *n* upon the dissociation

energy, U and dielectric constant ε can be understood through this relation ($n = n_o \exp(-U/\varepsilon' K T)$) [Ramya et al., 2008].

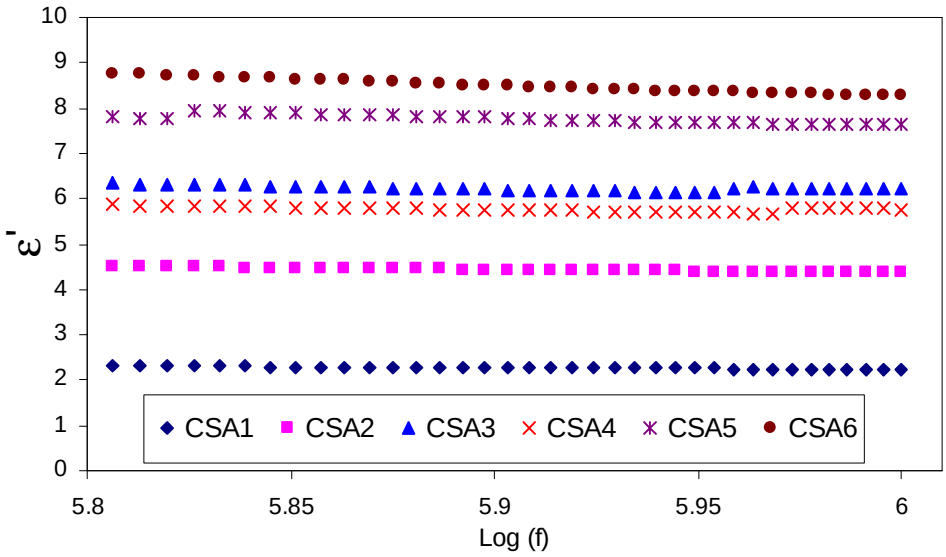

Figure 5.4 Composition dependence of bulk dielectric constant for chitosan-silver triflate SPEs at 303 K.

The increase in the value of dielectric constant upon the addition of $AgCF_3SO_3$ salt, indicates that there is an increase in charge carrier concentration as can be inferred from the equation ($n = n_o \exp(-U/K_B\varepsilon' T)$) assuming n_o and U are constant at the temperature considered. Hence an increase in polarization as well as DC conductivity ($\sigma = \Sigma qn\mu$) are expected. Thus, an increase in dielectric constant can imply an increase in charge carrier concentration according to the above relation and consequently an increase in DC conductivity. Fig. 5.5 shows the dependence of bulk dielectric constant and bulk DC conductivity on salt concentration. It can be seen that bulk dielectric constant and bulk DC conductivity follows similar trends with salt concentration. These results imply that DC conductivity and dielectric constant should be related to each other.

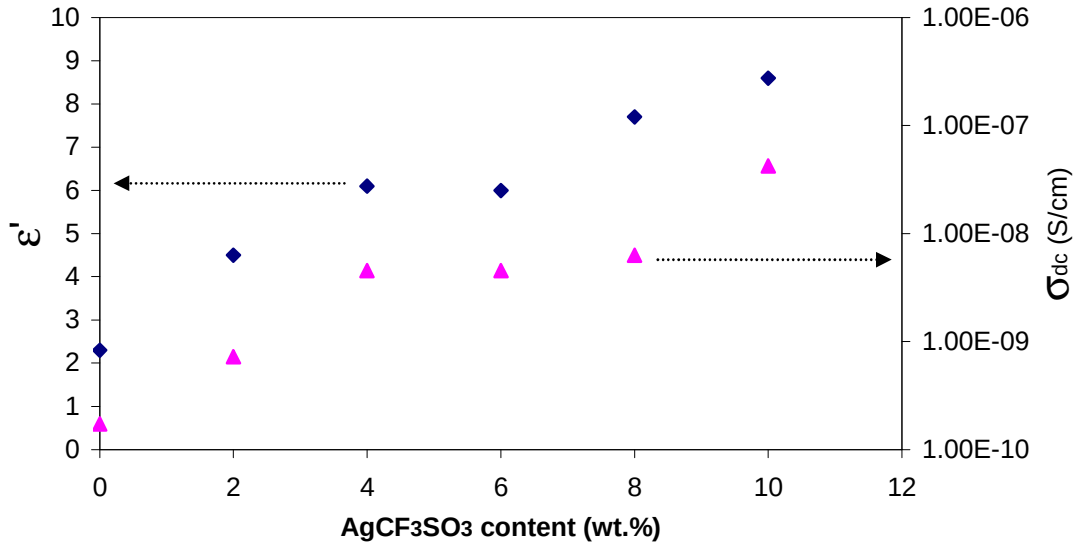

Figure 5.5 Bulk dielectric constant and DC conductivity as a function of AgTf salt concentration.

The above results indicate the fact that dielectric analysis is an informative technique to study conductivity behavior of polymer electrolytes. The frequency and temperature dependence study of dielectric constant may help to further understand the correlation between DC conductivity and dielectric constant.

Figure 5.6 shows the frequency dependence of dielectric constant for CSA6 at different temperatures. From the figure, it is seen that the dielectric constant decreases with increasing frequency. The high value of ε' at low frequencies is due to the enhanced charge carrier density at the electrolyte–electrode interface, i.e., due to the accumulation of charged species at the electrode/electrolyte interface [Nithya et al., 2010]. These high ε' values do not represent the materials properties; rather they represent the dielectric properties associated with the electrodes (electrode polarization effect). However, the high

frequency region of dielectric constant (Fig 5.7) which represents the material (bulk) properties is almost frequency independent but temperature dependent.

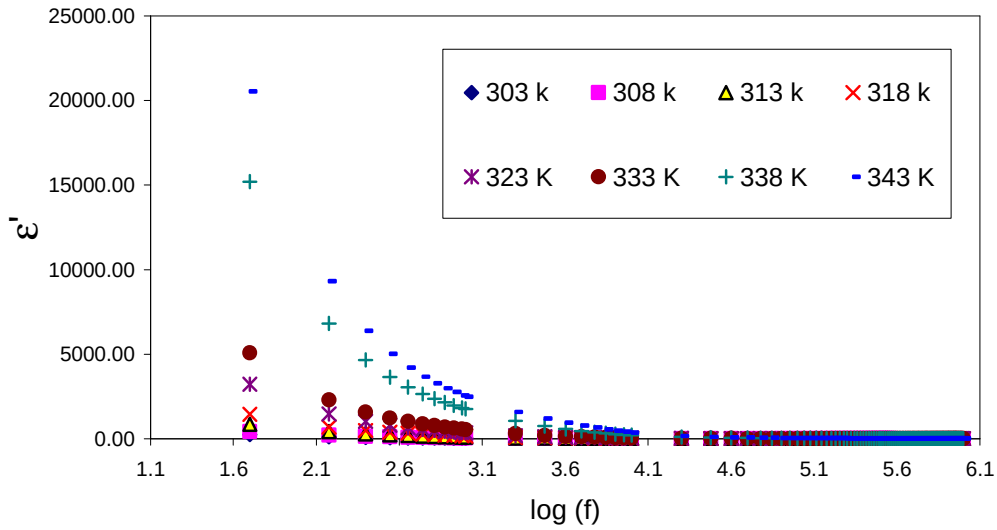

Figure 5.6 Frequency dependence of dielectric constant at different temperatures for CSA6 sample.

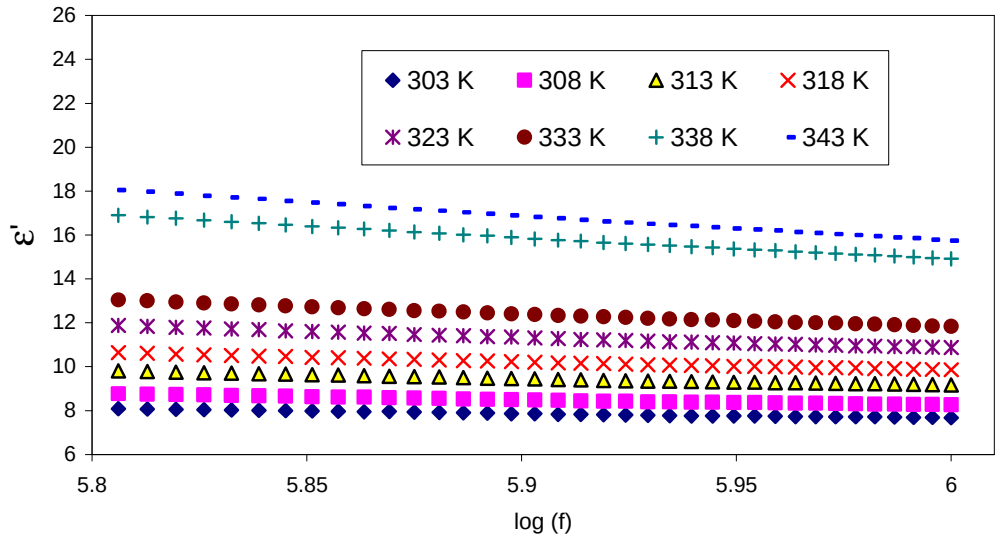

Figure 5.7 Frequency dependence of bulk dielectric constant at different temperatures for CSA6 sample.

The dielectric constants plateau from 303 to 338 K (Fig. 5.27) demonstrated in this work for the first time can be obtained only for low salt concentrations. At this juncture, we can make a conjunction between DC conductivity and dielectric constant as have been reported by Petrowsky and Frech (2009, 2010), because DC conductivity is also calculated from the high frequency semicircle (bulk properties).

Figure 5.8 shows the smooth curve between DC conductivity and dielectric constant at different temperatures. This smooth curve in the temperature range can be viewed as an empirical description of the σ_{dc} dependence on dielectric constant (ε′) at different temperatures [Petrowsky and Frech, 2009]. Thus it can be understood that an increase in dielectric constant can imply an increase in charge carrier concentration and consequently an increase in DC conductivity ($\sigma = \Sigma qn\mu$).

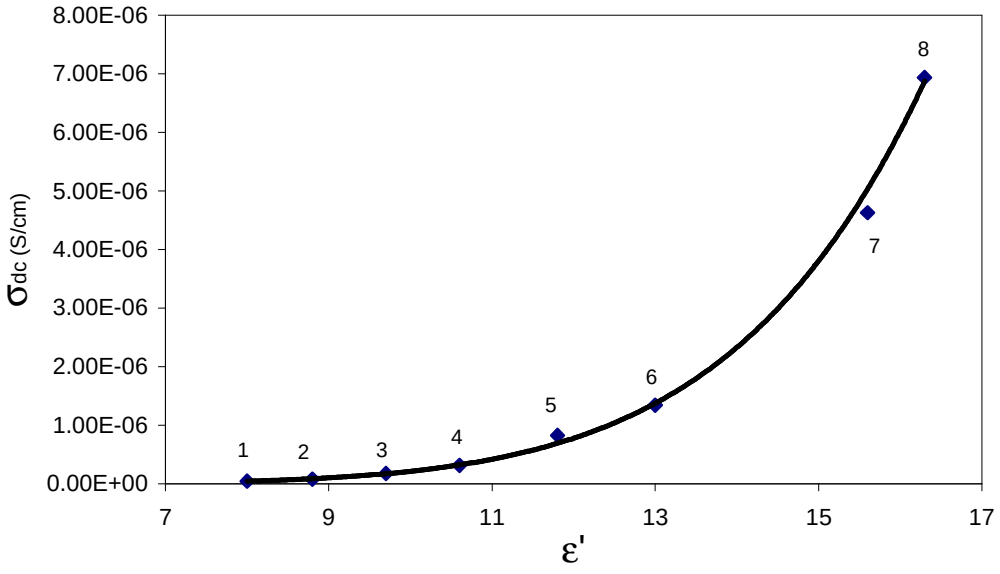

Figure 5.8 DC conductivity dependence on dielectric constant at, (1) 303, (2) 308, (3) 313, (4) 318, (5) 323, (6) 333, (7) 338and (8) 343 K for CSA6 sample.

The smooth curve (Fig. 5.7) together with the concentration dependence of DC conductivity on dielectric constant (Fig. 5.5) reveals a strong relationship between DC conductivity and dielectric constant in the present solid polymer electrolyte. These results indicate the fact that DC conductivity is not only a function of temperature as exhibited in Arrhenius equation ($\sigma_{dc}(T) = \sigma_o e^{-E_a / K_B T}$) but also a function of dielectric constant ($\sigma_{dc}(T, \varepsilon') = \sigma_o e^{-E_a / K_B T}$).

One point of conductivity can be selected on this curve (Figure 5.8) as a reference to scale the DC conductivity. Figure 5.9 demonstrates the compensated Arrhenius behavior for the temperature dependence of conductivity for CSA6 complex system scaled at a reference temperature of 333 K. It can be seen that the temperature dependence is linear with a regression value of 0.98. The slope gives activation energy of 1.127 eV, which is almost the same compared to that calculated from the normal Arrhenius relation.

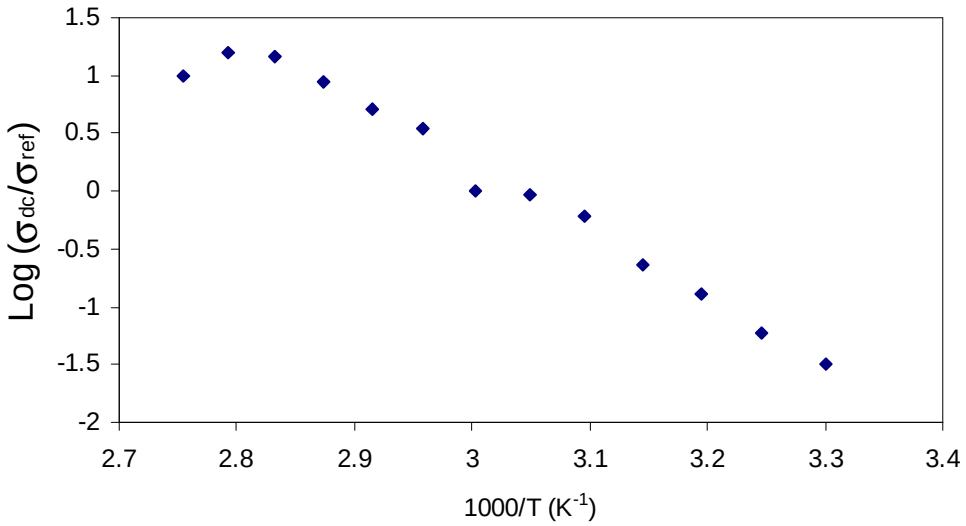

Figure 5.9 Compensated Arrhenius equation plotted against the reciprocal temperature for CSA6 system.

The calculated activation energy from the compensated Arrhenius plot was used to evaluate the pre-exponential factor by dividing the conductivity with the quantity $\exp(-E_a / K_b T)$, and is presented in Fig. 5.10. The results of Fig 5.10 are not followed the Petrowsky and Frech work (2009, 2010), which gives a smooth curve between pre-exponential factor and dielectric constant. It can be seen that the pre-exponential factor is almost randomly distributed with dielectric constant. The compensated Arrhenius behavior and the pre-exponential factor indicate the fact that solid electrolytes are following the normal Arrhenius behavior only. To improve the dependence of DC conductivity on dielectric constant in Arrhenius equation and the non-applicability of Petrowsky and Frech hypothesis for solid electrolyte another two systems were taken to study in which the cations cannot be reduced by chitosan.

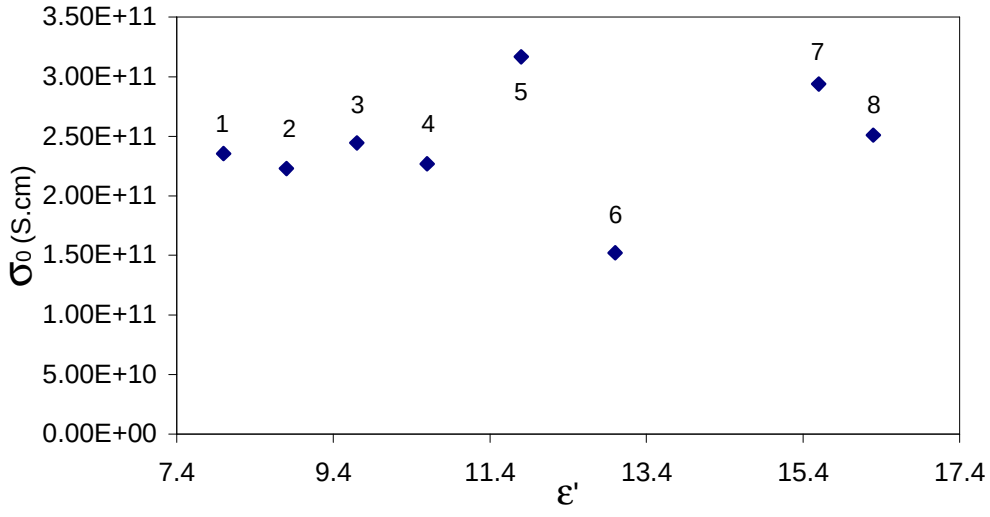

Figure 5.10 Temperature and dielectric constant dependent of pre-exponential factor (σ_o) at (1)303, (2) 308, (3) 313, (4) 318, (5) 323, (6) 333, (7) 338 and (8) 343 K for CSA6 system.

Figure 5.11 shows the frequency variation of dielectric loss at selected temperatures. It was observed that the dielectric loss exhibits high values at low frequencies attributable to charge accumulation. The large value of ε'' compared to ε' can be ascribed to the contribution of dipolar orientation, interfacial polarization and DC conductivity to ε'' ($\varepsilon'' = \varepsilon''_{dipo} + \varepsilon''_{inter} + \varepsilon''_{dc}$) values (Pradhan et al., 2008b). Here, ε''_{dipo} is dielectric loss due to dipolar orientation; ε''_{inter} is that due to interfacial polarization and ε''_{dc} is dielectric loss due to DC conductivity. The absence of relaxation peaks in dielectric loss spectra is also ascribed to DC contribution.

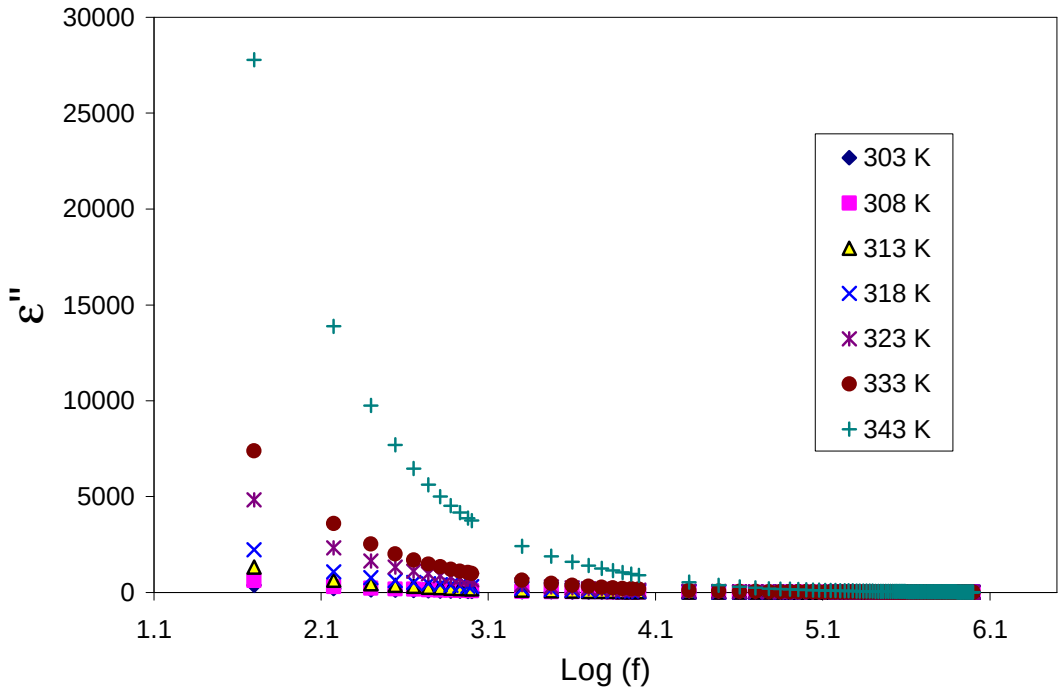

Figure 5.11 Frequency dependence of dielectric loss at different temperatures for CSA6 sample.

5.2.2 Frequency dependence of tan δ for CS:AgTf (CSA6) SPE

To obtain knowledge of the relaxation processes, tan δ was plotted as a function of frequency at different temperatures for SPE_6. It can be observed from Figure 5.12 that tan δ increases with frequency, passes through a maximum value and thereafter decreases. It is clear from the figure that the maximum of tan δ peaks $(\tan \delta)_{max}$ shifts to higher frequencies as the temperature increases which indicates the increase in ion conductivity. The loss peaks and their shifts with temperature suggest a dielectric relaxation process [Ravi et al., 2011].The frequency associated with each peak is known as relaxation frequency and gives the most probable relaxation time for ions from the relation $2\pi f_{max}=1/\tau$, τ is the relaxation time and f_{max} is the frequency corresponding to $(\tan\delta)_{max}$.

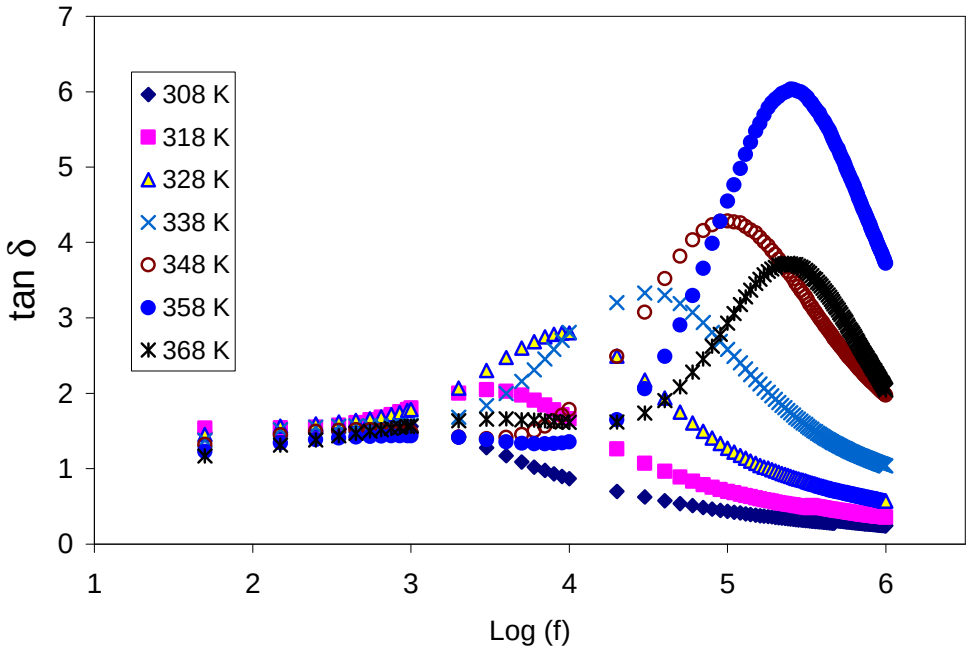

Figure 5.12 Frequency dependence of loss tangent (tanδ) at different temperatures for CSA6 sample.

The reciprocal temperature variation of log (f_{max}) is shown in Figure 5.13. The frequency-temperature relationship satisfies the Arrhenius behavior with the activation energy, E_a = 1.12 eV. This activation energy is very close to that one obtained from plots of Log (σ) against 1000/T (1.13 eV). This agreement between activation energy obtained from the tan δ peaks and DC conductivity may be due to the fact that an ion has to overcome the same barrier while conducting as well as while relaxing [Ahmed et al., 2003].

The rise in temperature causes the drop in relaxation time due to the increased mobility of ionic carriers which is temperature dependent. The regression value R^2 is 0.998 indicating that all points lie on an almost perfect straight line.

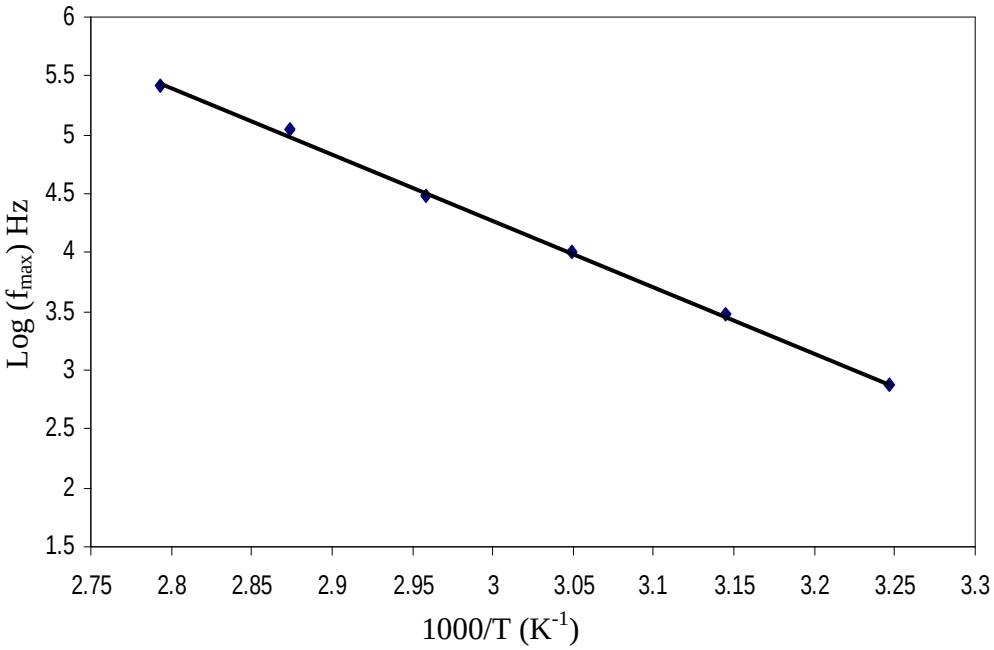

Figure 5.13 Temperature dependence of relaxation frequency for CSA6 sample.

5.2.3 Electric modulus analysis of CSA6: Relaxation processes

Figures 5.14 show the frequency dependence of real parts of complex modulus at several temperatures for the CSA6 sample. From Figure 5.14, it is obvious that at lower frequencies M' values tend to zero indicating the removal of electrode polarization, [Yakuphanoglu, 2007] while the increase of M' with increasing frequency and reaching a maximum value M_∞ at high frequency, may be due to the distribution of relaxation processes over a range of frequencies [Patro and Hariharan, 2009a].

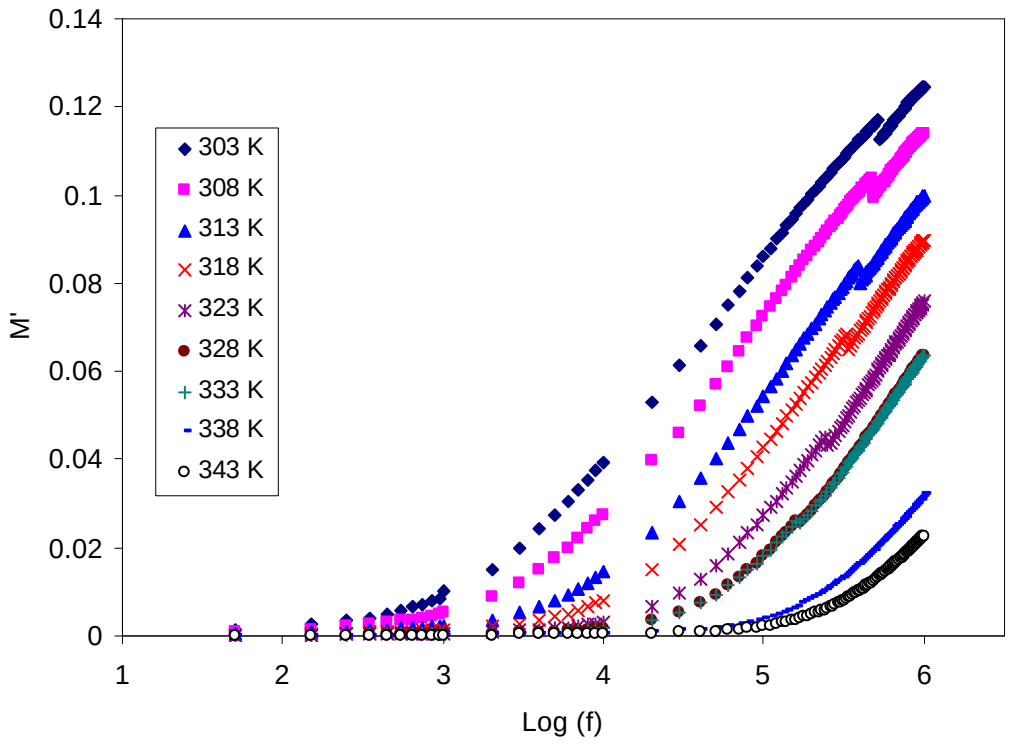

Figure 5.14 Frequency dependence of M′ at different temperature for chitosan-silver triflat (CSA6).

Figure 5.15 show the frequency dependence of M" at different temperatures for CSA6 sample. The appearance of loss peaks are clearly observed in Figure 5.15. It is obvious that at lower frequencies M" exhibits low value, which might be due to the large value of capacitance associated with the electrode polarization effect [Patro and Hariharan, 2009b]; as a result of accumulation of a large amount of charge carriers at the electrode/solid polymer electrolyte interface. However, at high frequencies well-defined peaks are observed.

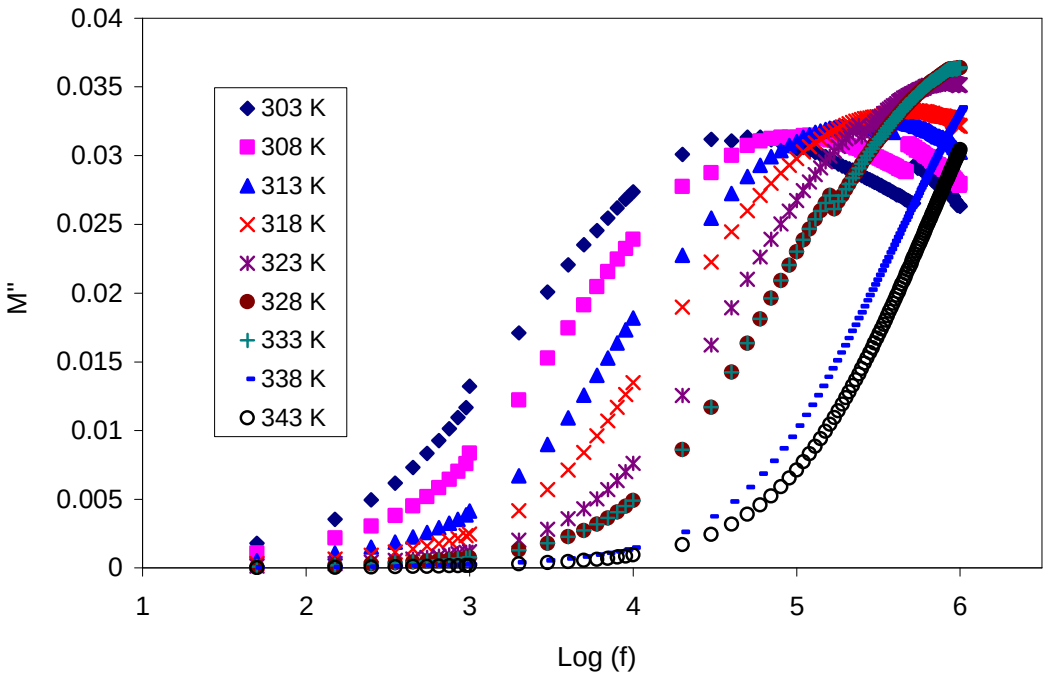

Figure 5.15 Frequency dependence of *M''* at different temperature for chitosan-silver triflate (CSA6).

The study of Argand plot at different temperatures can be used to demonstrate the nature of relaxation processes in the present polymer electrolyte. Figure 5.16 shows the temperature dependence of Argand plots. It is obvious from Figure 5.16, that the curves of Argand plots

are incomplete semicircle which cannot be explained by the Debye model (i.e., single relaxation time). It can be seen that with increasing temperature the Argand curves shifts towards the origin. This is can be ascribed to the increase in conductivity resulting from increasing ionic mobility with temperature and thus the decrease of both Z_r and Z_i.

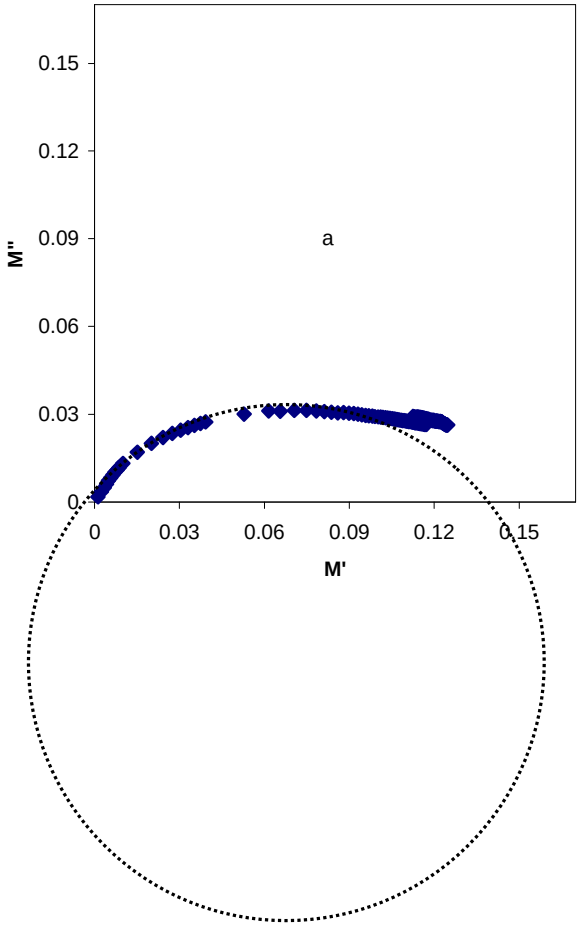

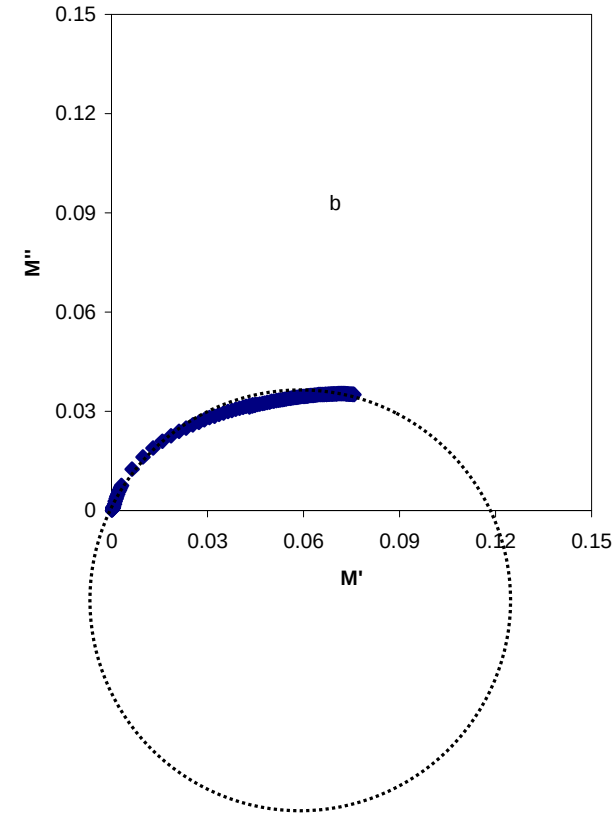
0.15
0.12
0.09
0.06
0.03
0
M''
b
0
0.03
0.06
0.09
0.12
0.15
M'

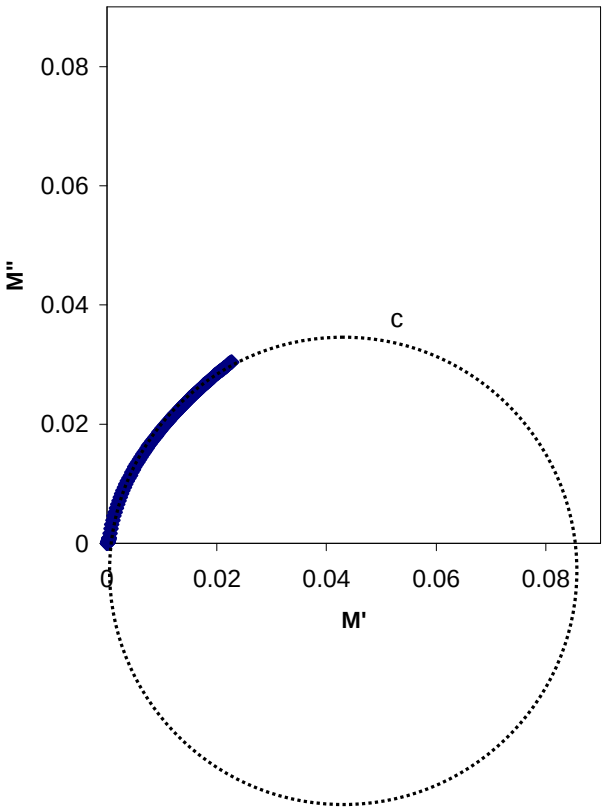
0.08
0.06
0.04
0.02
0
M''
c
0
0.02
0.04
0.06
0.08
M'

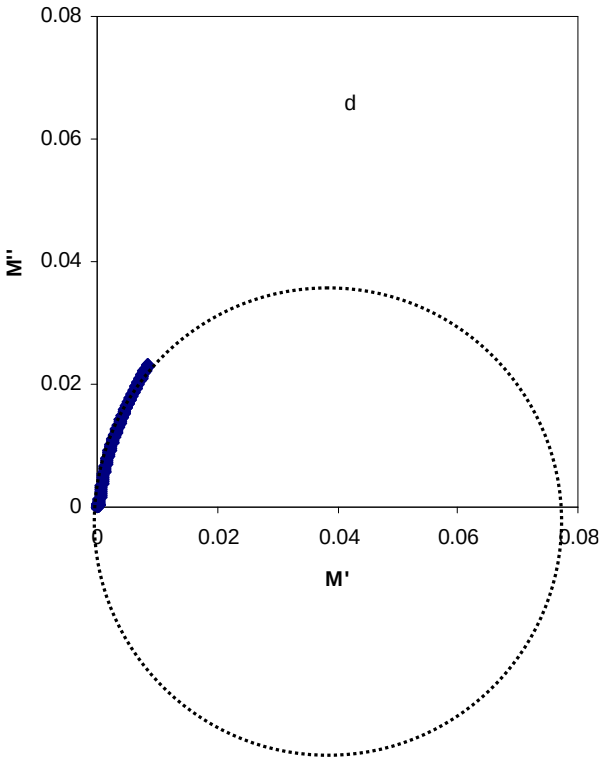

Figure 5.16 Argand plots for chitosan-silver triflate at (CSA6) at (a) 303 K, (b) 323 K, (c) 333 K and (d) 343 K.

5.2.4 Correlation between impedance and AC conductivity (σ_{ac}) of SPE based on CS:AgTf (CSA6)

The complex impedance plots at different temperatures shown in Figure 5.17, strongly support the above explanation for the increase of M' and M''. The complex impedance plots (Z_i vs Z_r) are commonly used to separate the bulk material (depressed semicircle) and the electrode surface polarization phenomena (tilted spike) [Sengwa et al., 2008b]. The electrode polarization phenomena (tilted spike) occurs due to formation of electric double layer (EDL) capacitances by the free charges build up at the interface between the electrolyte and the electrode surfaces in plane geometry [Aziz et al., 2010b]. The

appearance of second semicircle at different temperatures in the intermediate frequencies can be attributed to silver nanoparticle that acts as grain boundaries in the present system (Fig. 5.17) especially at higher temperatures a distinguishable second semicircle is observed. It can be seen that the high frequency semicircle which corresponds to ionic conduction (bulk) decreases with increase in temperature and almost disappear at high temperatures while the second semicircle which correspond to silver nanoparticles grows with increasing temperature. These results support the DC conductivity-temperature relationship, i. e., the drop in DC conductivity at higher temperatures (Fig. 5.2) can be ascribed to the reduction of silver ions to silver nanoparticles. The UV-vis and XRD results at different temperatures in Chapter Four reveal that the reductions of silver ions to silver nanoparticles are temperature dependent. It can be noticed that the electrode polarization region (spike region) is increased with increasing temperature due to the increase of charge accumulation at the electrode/electrolyte interface.

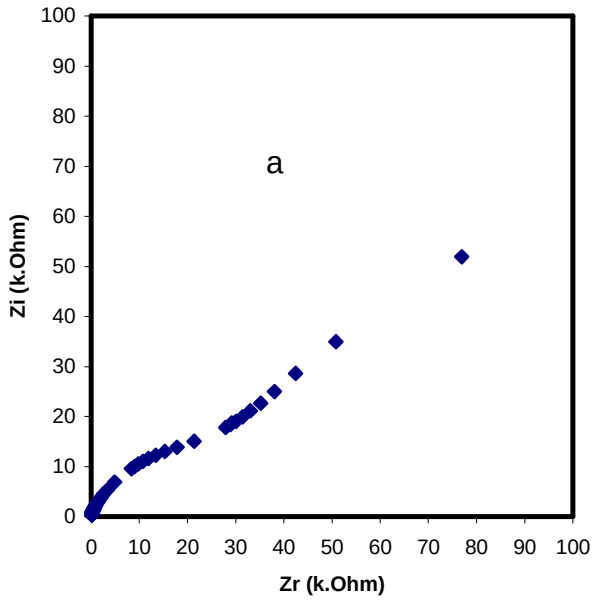

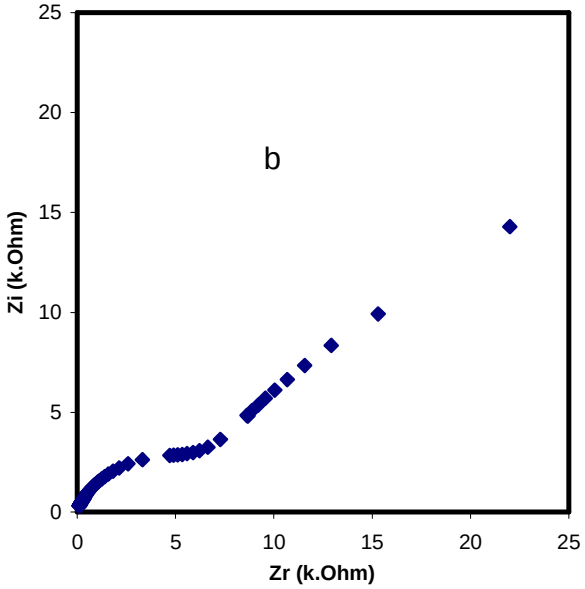
b
Zi (k.Ohm)
Zr (k.Ohm)
0
5
10
15
20
25

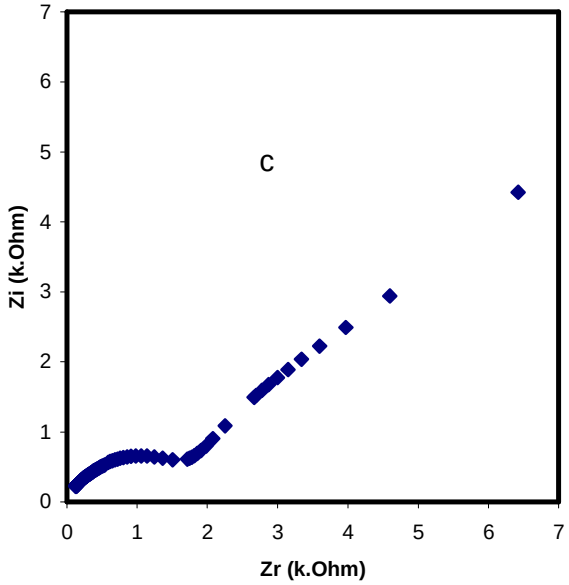
c
Zi (k.Ohm)
Zr (k.Ohm)
0
1
2
3
4
5
6
7

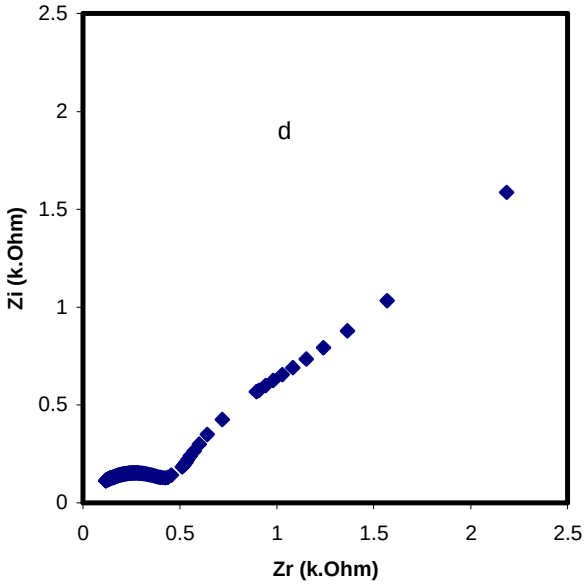
d
Zi (k.Ohm)
Zr (k.Ohm)
0
0.5
1
1.5
2
2.5

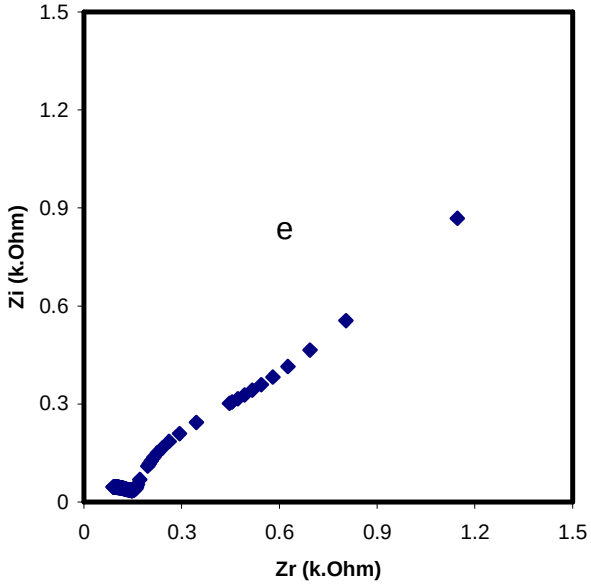
e
Zi (k.Ohm)
Zr (k.Ohm)
0
0.3
0.6
0.9
1.2
1.5

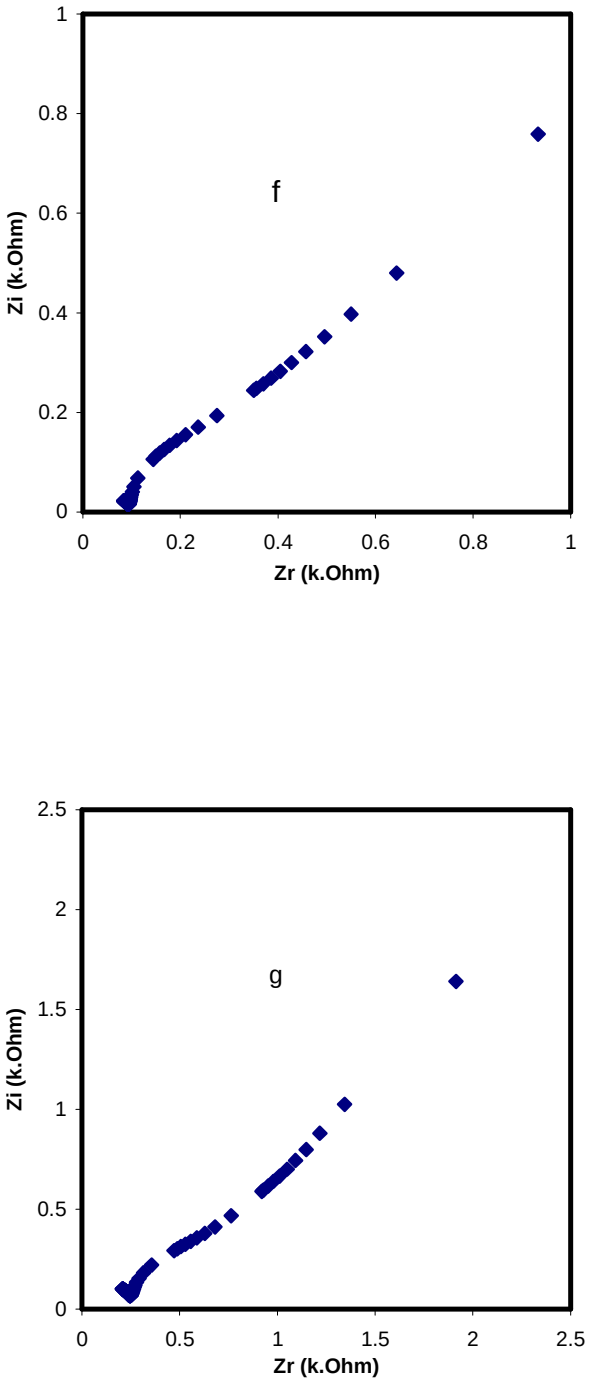

Figure 5.17 Impedance plots of chitosan:$AgCF_3SO_3$ (CSA6) at (a) 308 K, (b) 318 K, (c) 328 K, (d) 338 K, (e) 348 K, (f) 358 K and (g) 368 K.

In order to understand the nature of ion conduction in polymer electrolytes, the frequency dependence of ac conductivity at various temperatures has been analyzed for the highest conducting sample (CSA6) and presented in Fig. 5.18. The observed ac conductivity spectra from Fig. 5.18 (a) to 5.18 (d) exhibit three distinct regions. The low frequency data points region (I) is attributable to electrode polarization [Suman et al., 2006]. The points in region (II) which are quite frequency independent can be ascribed to the bulk DC conductivity, and data in the high frequency region (III) are due to conductivity dispersion that shift to high frequency with increasing temperature. The decrease of dispersion region with temperature is directly related to the disappearance of high frequency semicircle in impedance plots (Z_i-Z_r) at higher temperatures. These results indicate a good correlation between impedance analysis and ac conductivity dispersion. These dispersion regions are very important to characterize the type of ion conduction in solid polymer electrolytes by calculating the frequency exponent (s). The decrease of ac conductivity at 368 K (Fig. 5.18(g)) can be ascribed to the reduction of silver ion to silver nanoparticles.

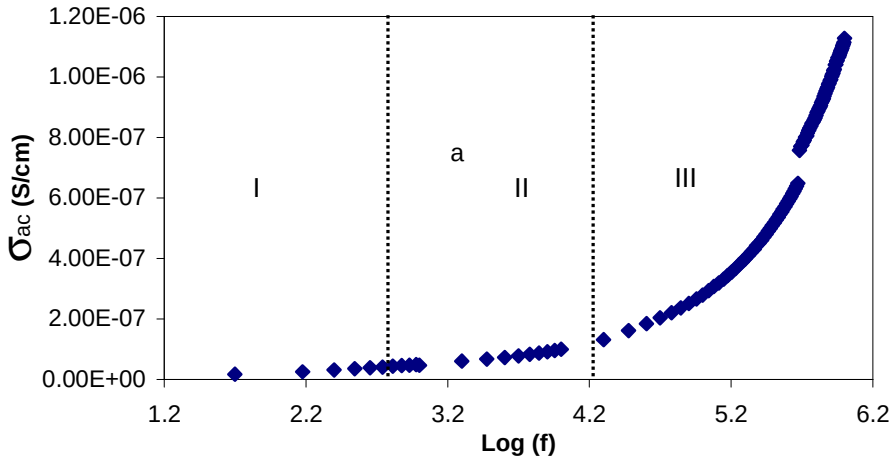

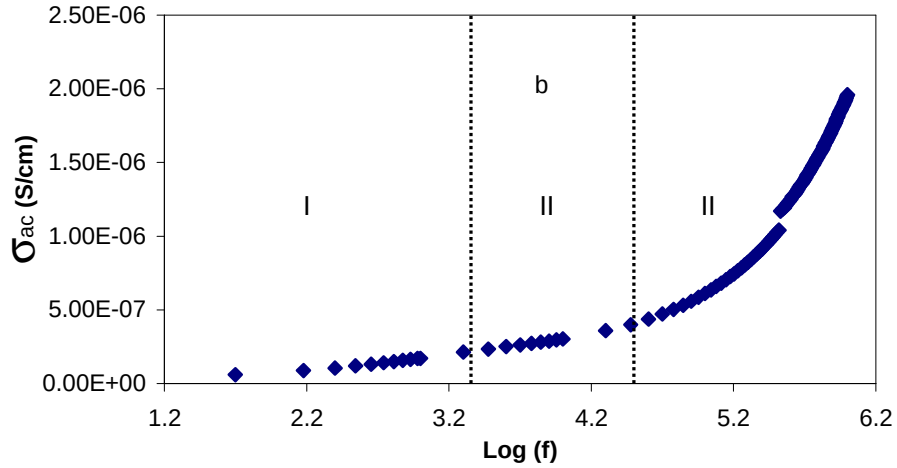
2.50E-06
2.00E-06
1.50E-06
1.00E-06
5.00E-07
0.00E+00
σac (S/cm)
b
I
II
II
1.2
2.2
3.2
4.2
5.2
6.2
Log (f)

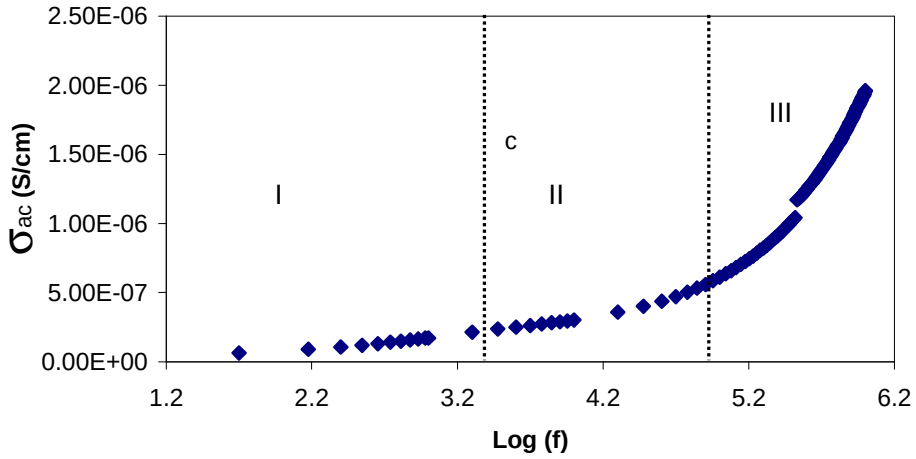
2.50E-06
2.00E-06
1.50E-06
1.00E-06
5.00E-07
0.00E+00
σac (S/cm)
c
I
II
III
1.2
2.2
3.2
4.2
5.2
6.2
Log (f)

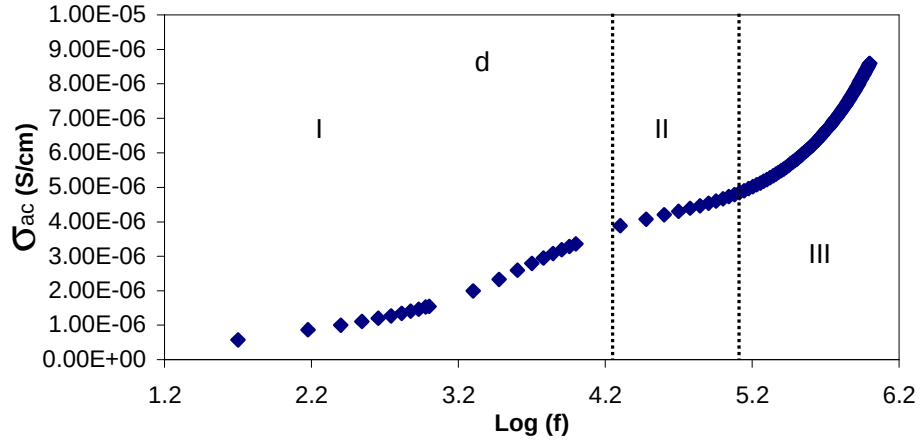
1.00E-05
9.00E-06
8.00E-06
7.00E-06
6.00E-06
5.00E-06
4.00E-06
3.00E-06
2.00E-06
1.00E-06
0.00E+00
σac (S/cm)
d
I
II
III
1.2
2.2
3.2
4.2
5.2
6.2
Log (f)

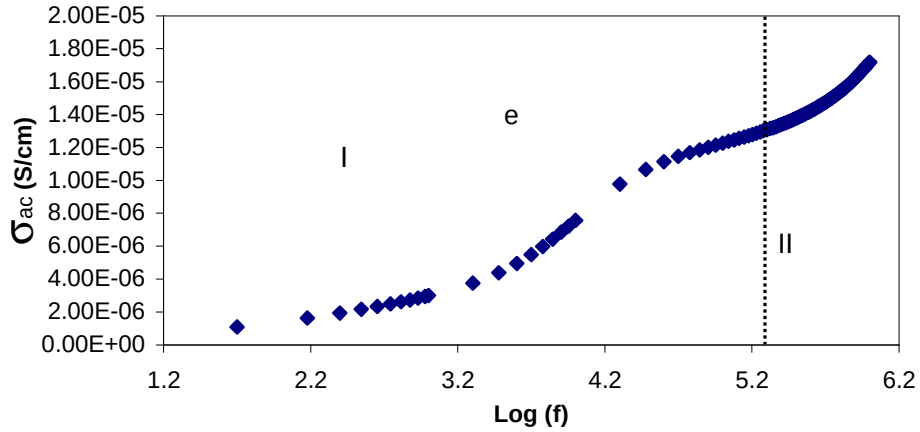
2.00E-05
1.80E-05
1.60E-05
1.40E-05
1.20E-05
1.00E-05
8.00E-06
6.00E-06
4.00E-06
2.00E-06
0.00E+00
σac (S/cm)
e
I
II
1.2
2.2
3.2
4.2
5.2
6.2
Log (f)

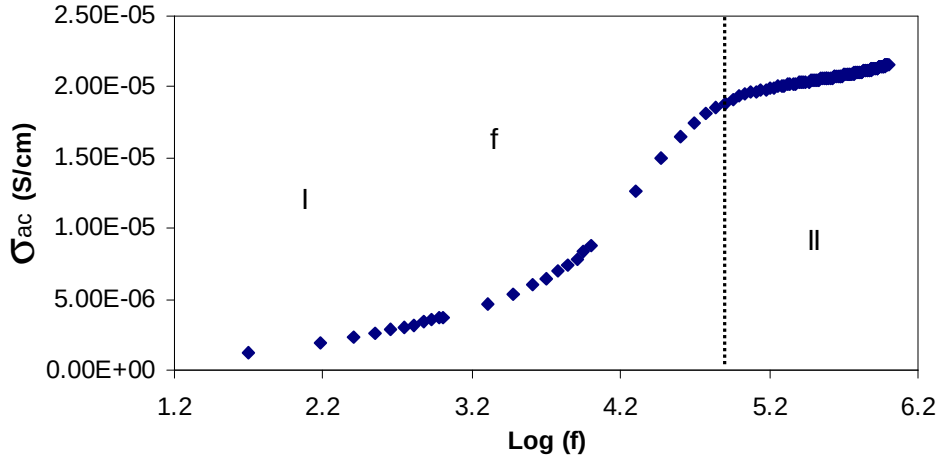
2.50E-05
2.00E-05
1.50E-05
1.00E-05
5.00E-06
0.00E+00
σac (S/cm)
f
I
II
1.2
2.2
3.2
4.2
5.2
6.2
Log (f)

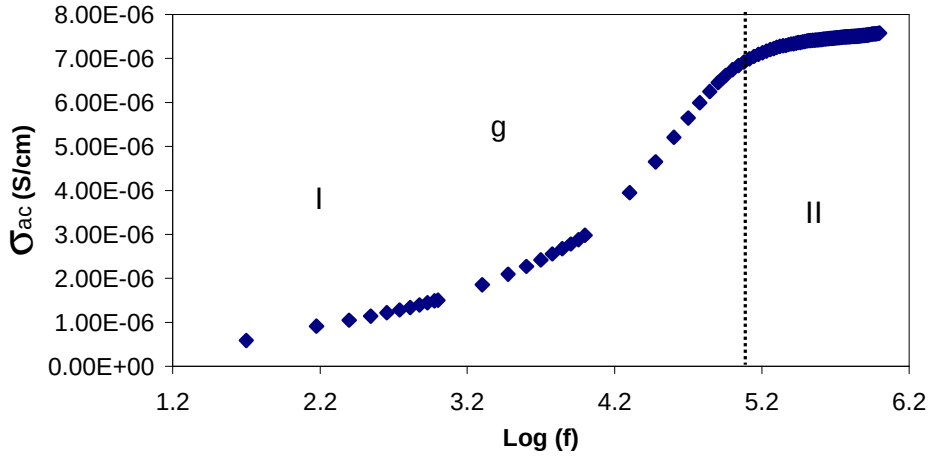

Figure 5.18 AC conductivity spectra of chitosan:$AgCF_3SO_3$ (CSA6) at (a) 308 K, (b) 318 K, (c) 328 K, (d) 338 K, (e) 348 K, (f) 358 K and (g) 368 K.

In general the obtained ac conductivity results indicate that the ac conductivity obeys the Jonschers power law [Baskaran et al., 2006]:

$$\sigma = \sigma_{dc} + A\omega^{s}, \qquad 0 < s < 1 \qquad (3.2)$$

where σ_{dc} is the frequency independent dc conductivity, A is a temperature-dependent constant, and s is an exponent that indicates the increase or decrease of conductivity. The Jonschers power law widely observed in disordered materials like ionically conducting glasses, conducting polymers and also doped crystalline solids [Pradhan et al., 2008b]. The Jonschers power law can be explained on the basis of jump relaxation model (physical

model). Jump relaxation model (physical model) was developed for structurally disordered ionic conductors in order to rationalize the observed frequency dispersion. According to jump relaxation model, at very low frequencies an ion can jump from one site to its neighboring vacant site successfully contributing to the dc conductivity. At higher frequencies, the probability for the ion to go back again to its initial site increases due to the short time periods available. This high probability for the correlated forward-backward hopping at higher frequencies together with the relaxation of ions is responsible for the observed high frequency conductivity dispersion [Pradhan et al., 2008a]. The electrical conduction mechanism in different materials can be characterized by the frequency exponent *s* value and the behavior of *s* value can be explained by many theoretical models. The XRD results for SPEs and NCPEs (Chapter Four) reveal that the samples are almost amorphous, i. e., the samples are almost disorder ionic conductors. Thus the Jonschers power law can be studied.

The exponent *s* values were calculated from the slope of $\log(\sigma_{ac})$ versus $\log(\omega)$ at the frequency dispersion regions for different temperatures and presented in Fig 5.19. It is clear that initially the value of s decreases with increasing temperature (Region, I) to a minimum value and then increasing with increasing temperature (Region, II). The decrease in s values from 303 K to 363 K indicates that the correlated barrier hopping conductivity is dominant in ac conductivity mechanism. According to correlated barrier hopping (CBH) model [Migahed et al., 2004], the frequency exponent s is found to decrease with increasing temperature as depicted in Fig. 5.19. The application of CBH model can be observed in rigid solid polymer electrolytes. It was reported that in the rigid solid polymer electrolyte with highly polar functional group, ion can be transported by hopping mechanism between polar functional groups, which decoupled from the polymer segmental motion [Uno et al.,

2008]. However, the increase of s value (II) with increasing temperature above 363K can be explained based on small polaron (SP) hopping. According to small polaron (SP) hopping model [Farid and Bekheet, 2000], the s value increases with increasing temperature.

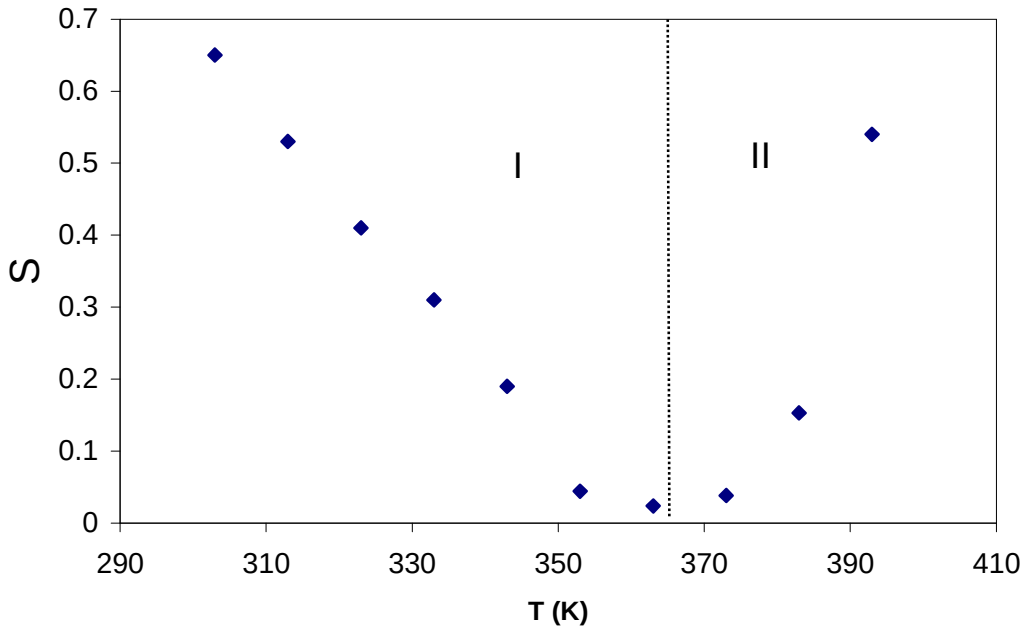

Figure 5.19 Temperature dependence of the frequency exponent s for CSA6 sample.

5.3 Electrical/Dielectric properties of SPEs based on CS:NaTf

5.3.1 DC conductivity and Dielectric analysis of SPE based on CS:NaTf

Figure 5.20 shows the variation of bulk DC conductivity with NaTf salt concentration. It can be seen that the ionic conductivity (Fig. 5.20) increased with increasing salt concentration. This shows that the ionic conductivity is almost governed by charge carrier

density at room temperature. The almost constant value of DC conductivity from 4 wt.% to 6 wt.% can be attributable to the almost similar rates between ion dissociation and ion association.

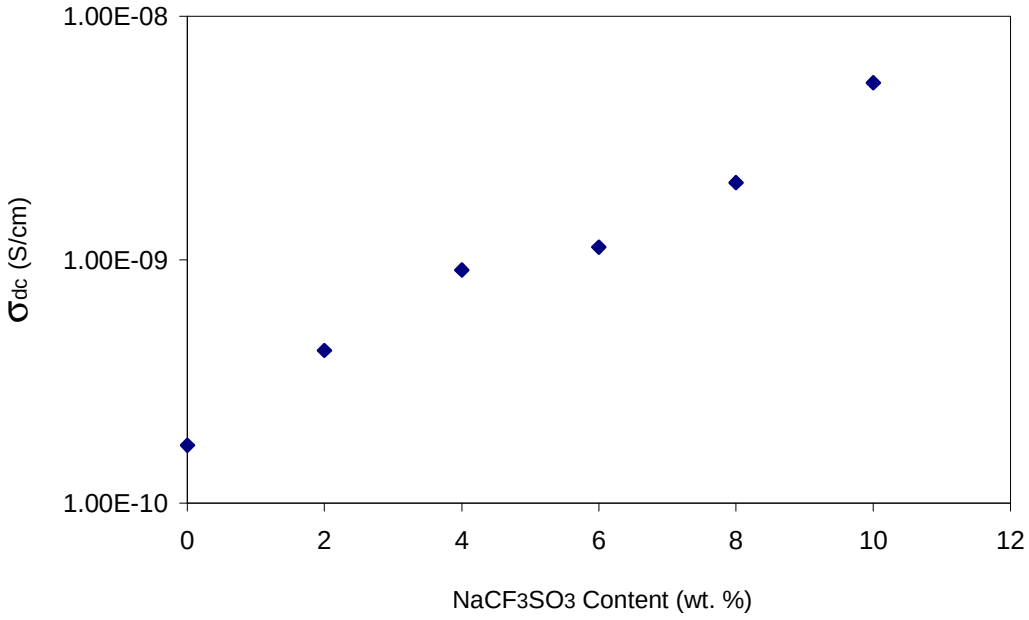

Figure 5.20 DC conductivity as a function of $NaCF_3SO_3$ concentration.

Figure 5.21 shows the temperature variation of DC conductivity for various salt concentrations. It is obvious that the DC conductivity increases almost linearly with rise in temperature in the low temperature region (region I). The linear relations which are observed in all chitosan:$NaCF_3SO_3$ compositions in region I indicate that there is no phase transition in the polymer electrolyte [Selvasekarapandian et al., 2005], i.e., the temperature dependence of ionic conductivity in the low temperature region is of the Arrhenius type.

The calculated E_a value for the highest conducting sample is 1.2 eV. However, the drop of dc conductivity at higher temperatures in region II can be attributed to the desorption of water (Aziz et al., 2010a).

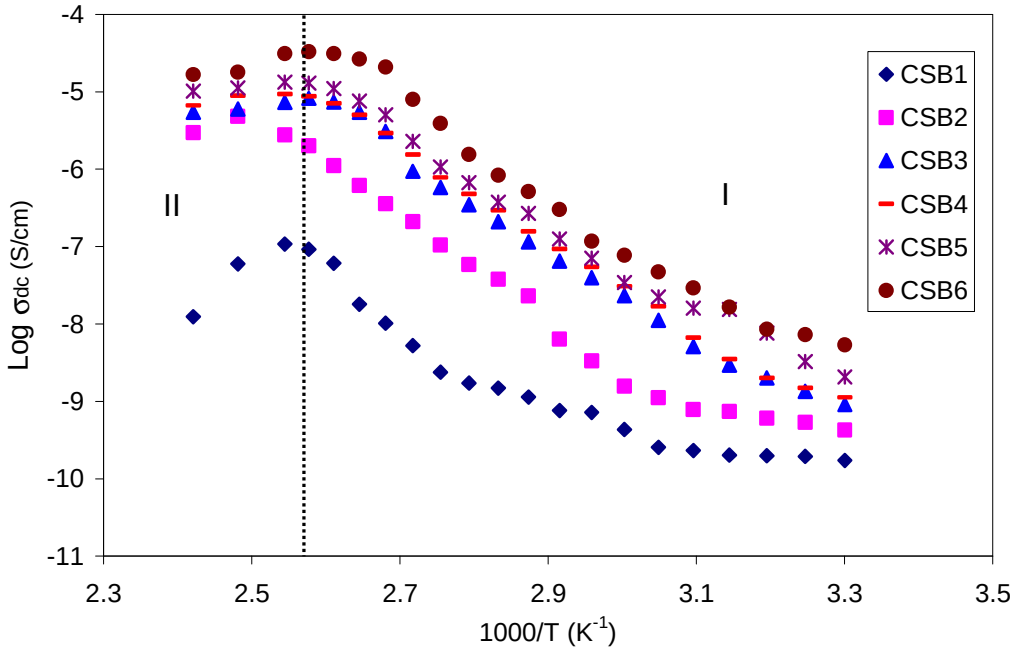

Figure 5.21 Temperature dependence of ionic conductivity for chitosan:NaTf complexes.

To correlate the DC conductivity with dielectric constant the composition and temperature dependence, dielectric constant was studied. Fig. 5.22 shows the variation of dielectric constant as a function of salt concentration at 303 K. It can be seen that at a fixed frequency, ε' increases with increase in salt concentration. In other words, the presence of salt at certain concentrations causes an increase in the value of dielectric constant. The low-

frequency dispersion region is attributed to the contribution of charge accumulation at the electrode/ electrolyte interface [Selvasekarapandian et al., 2005]. These values do not correspond to the bulk dielectric processes but they are rather due to the free charges that build up at the interface between the material and the electrodes.

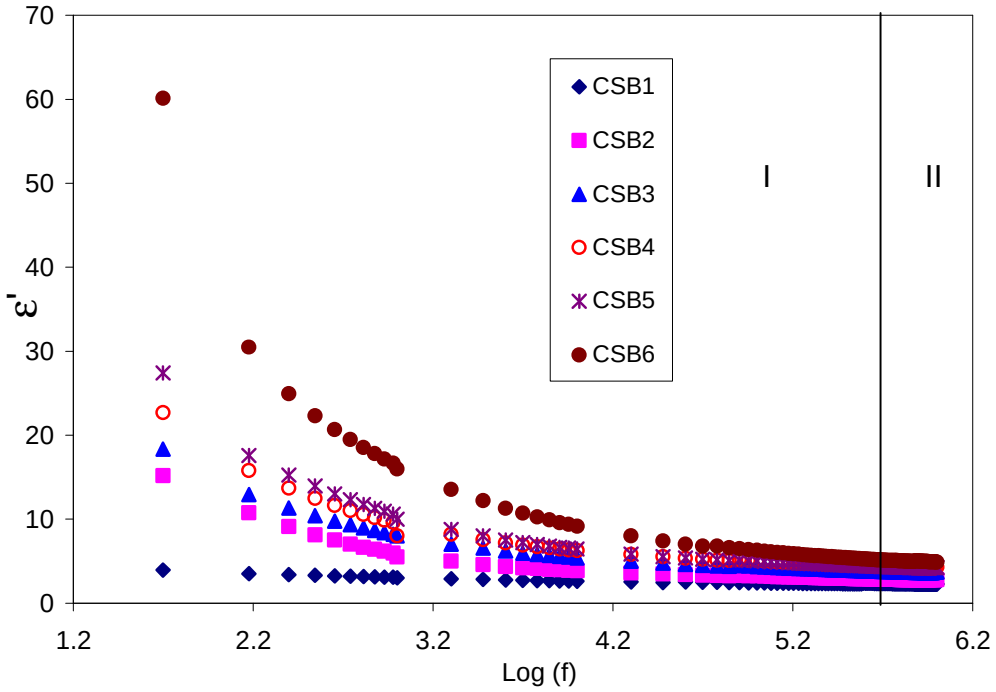

Figure 5.22 Compositional dependence of dielectric constant for CS:NaTf complexes.

The high frequency ε' values appear as a single curve as depicted in Fig.5.22, as a result of electrode polarization suppression. The high frequency dielectric constant is important because it represents ion conduction process in the bulk of polymer electrolytes [Hema et al., 2009c], and is also affected by salt concentration as shown in Fig. 5.23. It can be observed that the highest dielectric constant is obtained for 10 wt. % of sodium triflate,

due to the existence of highest concentration of free ions which is in good agreement with the XRD results which gives the lowest crystallite size for CSB6 sample (Chapter Four). Thus CS:NaTf exhibits similar behavior like CS:AgTf with salt concentration.

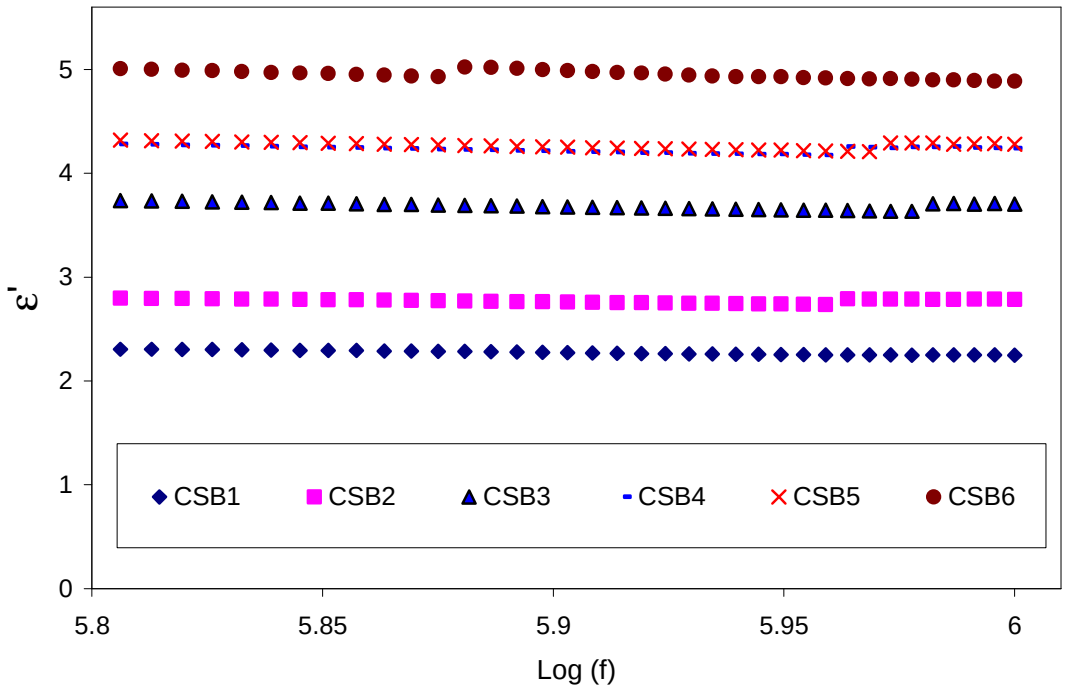

Figure 5.23 Compositional dependence of bulk dielectric constant for CS:NaTf complexes.

It can be seen that the bulk dielectric constant exhibits similar behavior with salt concentration like DC conductivity. The above results indicate the fact that dielectric analysis is an informative technique to study conductivity behavior of polymer electrolytes. The correlation between bulk DC conductivity and bulk dielectric constant can be

understood from Fig. 5.24. It can be seen that the bulk dielectric constant and bulk DC conductivity follows the same trend with NaTf salt concentration.

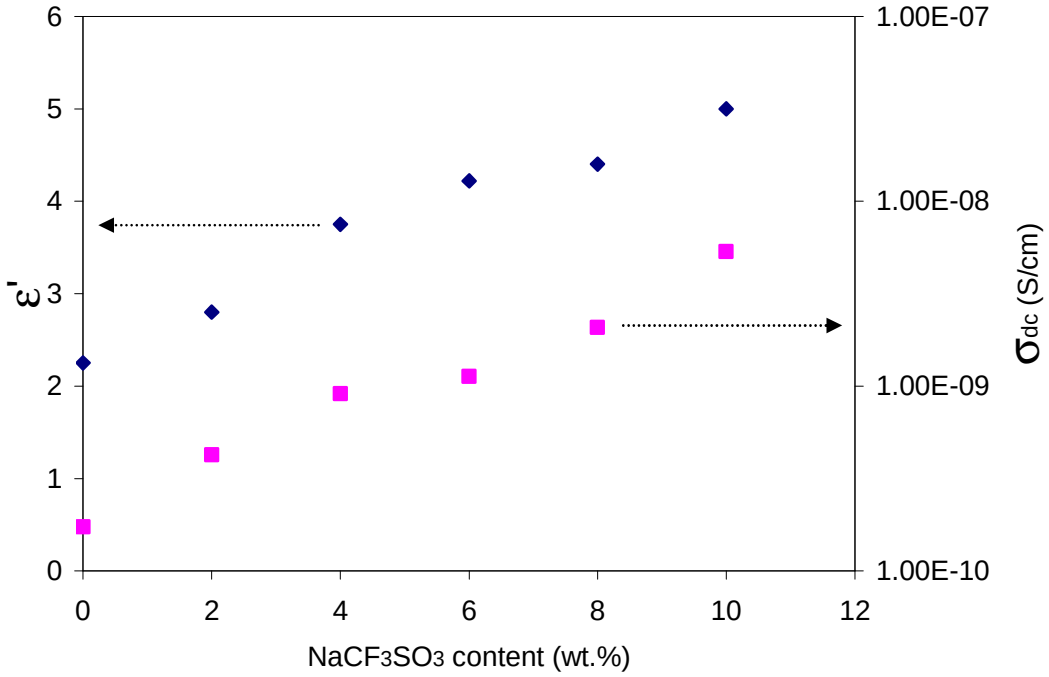

Figure 5.24 Variation of bulk dielectric constant and DC conductivity with various NaTf concentrations.

The conductivity behavior of polymer electrolytes can be understood from dielectric analysis. The dielectric constant is a measure of stored charge, i.e., directly related to the charge carriers [Kumar and Bhat, 2009]. The temperature dependence analysis of dielectric parameters may give further information between dielectric constant and DC conductivity.

Figure 5.25 shows the variation of dielectric constant with frequency at different temperatures for chitosan-$NaCF_3SO_3$ (CSB6). It can be seen that the high frequency values of dielectric constant correspond to the charge transfer process, i.e. to the bulk properties of the sample [Hema et al., 2009a], are also temperature dependent as shown in Fig.5.26.

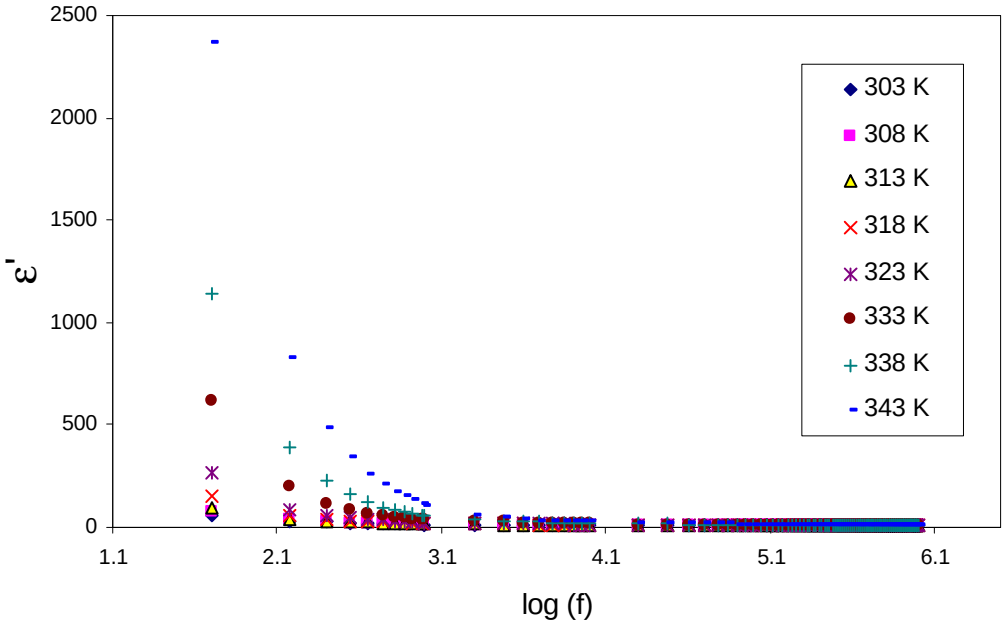

Figure 5.25 Frequency dependence of dielectric constant (ε′) for CSB6, at different temperatures.

The increase in bulk dielectric constant means an increase in the bulk DC conductivity of the sample. From this relation, $\varepsilon' = Q \times (d / V\varepsilon_o A) = cons\tan t \times Q$ (Q is total charge per area), it is understood that an increase in ε′, implies an increase in the fraction of the charge carriers.

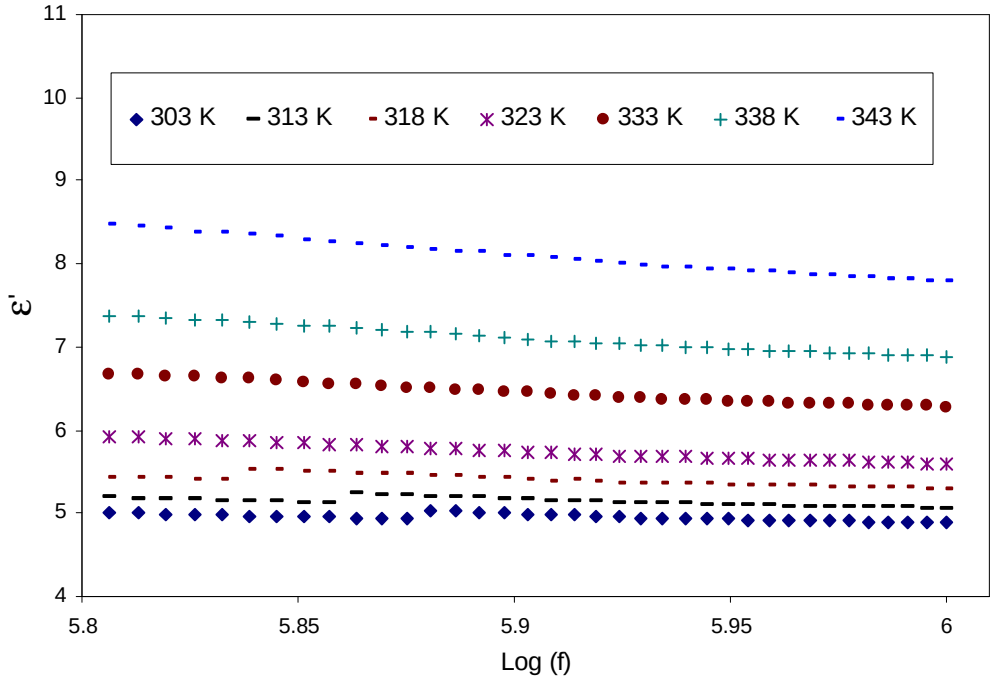

Figure 5.26 Frequency dependence of bulk dielectric constant (ε′) for CSB6 sample, at different temperatures

Figure 5.27 shows the smooth curve between DC conductivity and dielectric constant at different temperatures. The DC conductivity and bulk dielectric values were obtained from the bulk high semicircle of impedance plots. This smooth curve can be viewed as an empirical description of the dependence of σ on the dielectric constant (ε′) at different temperatures [Petrowsky and Frech, 2009]. This smooth curve indicate the fact that the increase in DC conductivity is due to the increase in dielectric constant and the increase in dielectric constant means an increase in charge carrier density. Thus the concentration dependence of DC conductivity and dielectric constant (Fig. 5.24) and temperature

dependence of DC conductivity and dielectric constant (Fig. 5.27) clearly reveal the dependence of DC conductivity on dielectric constant in Arrhenius equation.

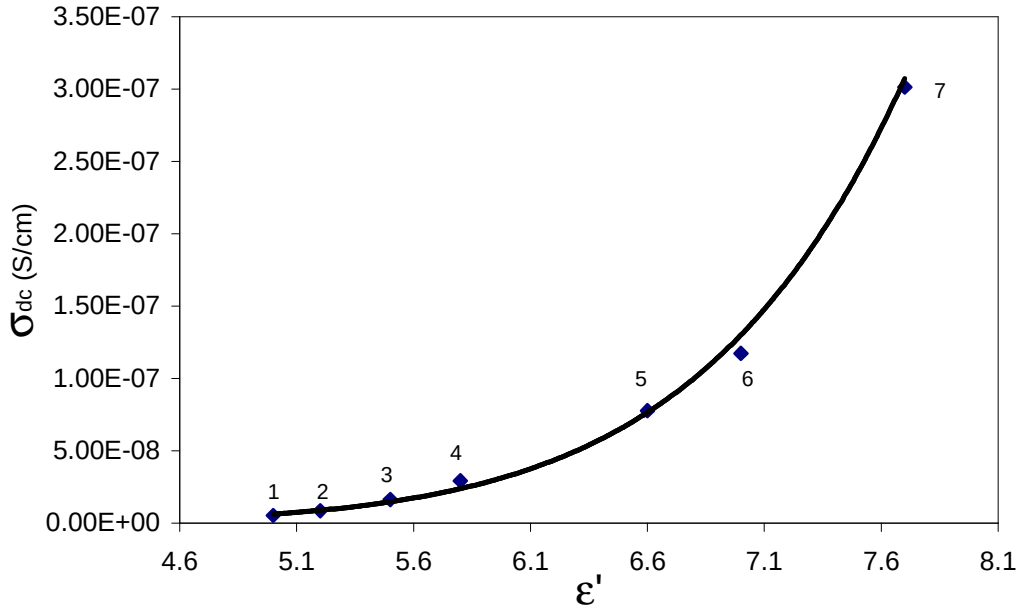

Figure 5.27 DC conductivity dependence on dielectric constant at, (1) 303, (2) 313, (3) 318, (4) 323, (5) 333, (6) 338 and (7) 343 K for CSB6 system.

One point of conductivity can be selected on this curve as a reference to scale the DC conductivity. Figure 5.28 demonstrates the compensated Arrhenius behavior for the temperature dependence of conductivity for CSB6 complex system scaled at a reference temperature of 333 K. It can be seen that the temperature dependence is linear in the low temperature region (Region, I) as observed for normal Arrhenius in Fig 5.21. The slope gives an activation energy of 1.18 which is almost the same compared to the calculated one from normal Arrhenius relation.

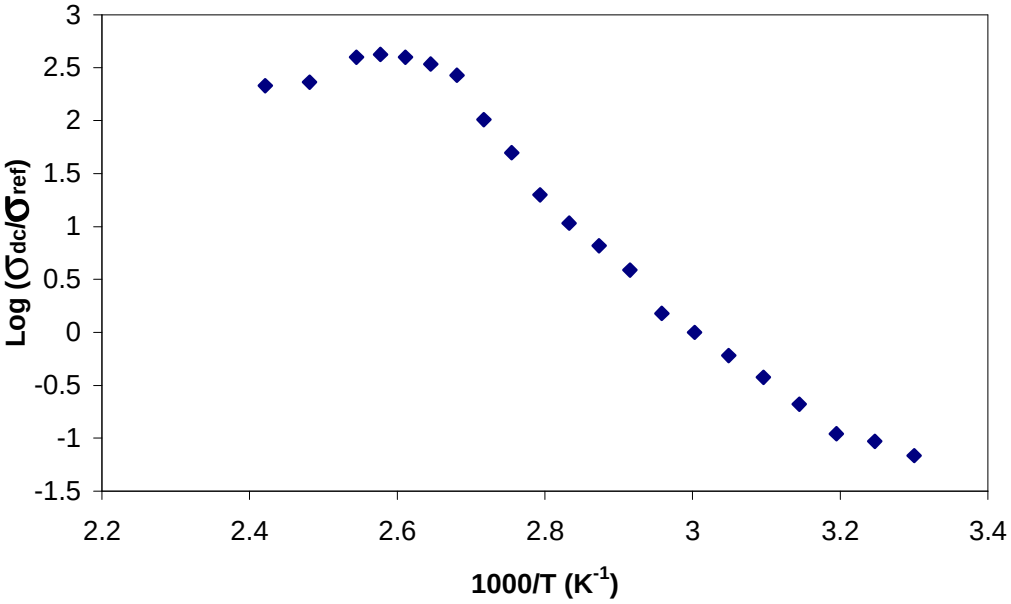

Figure 5.28 Compensated Arrhenius equation plotted against the reciprocal temperature for CSB6 system.

The calculated activation energy from the compensated Arrhenius plot was used to evaluate the pre-exponential factor by dividing the conductivity with the quantity $\exp(-E_a/K_bT)$, and is presented in Fig. 5.29. The results of Fig 5.29 are again like CS:AgTf system in contradiction with the Petrowsky and Frech work (2009, 2010), which gives a smooth curve between pre-exponential factor and dielectric constant. Thus the Petrowsky and Frech hypothesis also not applicable for the second SPE system, i.e., the SPEs follow the normal Arrhenius behavior with constant pre-exponential factor. This can also be understood from the comparison of Arrhenius and compensated Arrhenius figures which are almost the same with no distinguishable differences. These results strongly support the temperature

independence of pre-exponential factor (σ_o) in Arrhenius equation as depicted in Fig. 5.29 for CSB6 system.

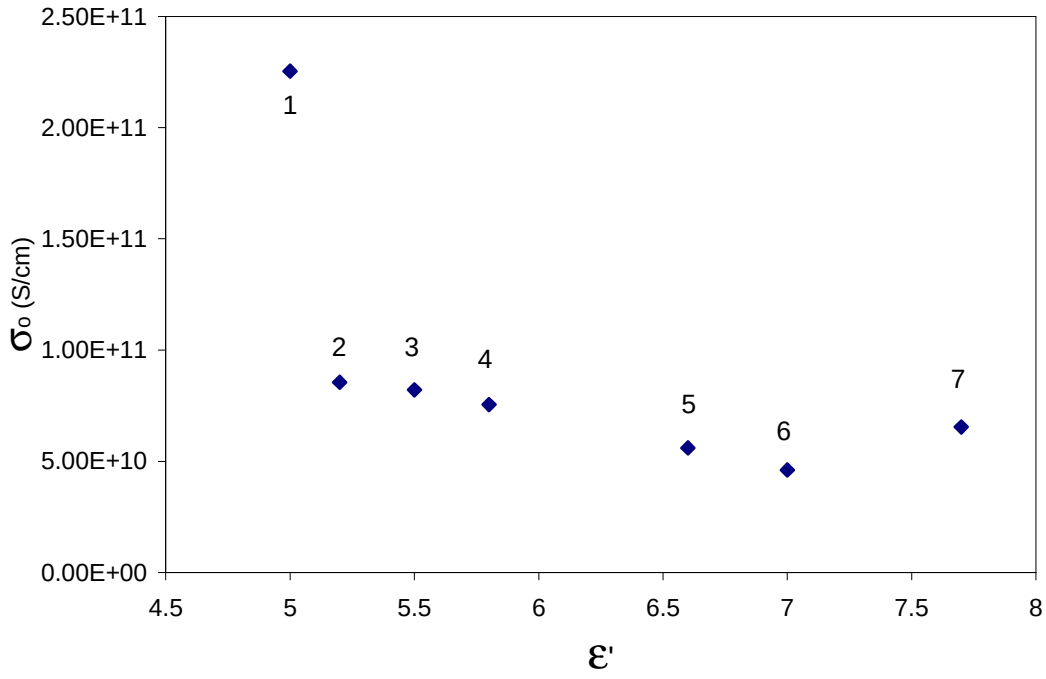

Figure 5.29 Temperature and dielectric constant dependent of pre-exponential factor (σ_o) at (1) 303, (2) 313, (3) 318, (4) 323, (5) 333, (6) 338 and (7) 343 K for CSB6 system.

Figure 5.30 shows the frequency dependence of dielectric loss for CSB6. At low frequencies, due to the long period and thus slow reversal of the electrical field, the mobile ions tend to accumulate at the electrode/electrolyte interface. This gives a high value of dielectric loss (ε″). On the other hand, at high frequencies, periodic reversal of the electric field occurs so fast that there is no excess ion diffusion in the direction of the field.

Polarization due to charge accumulation decreases, leading to the observed decrease in dielectric loss [Reddy et al., 2005].

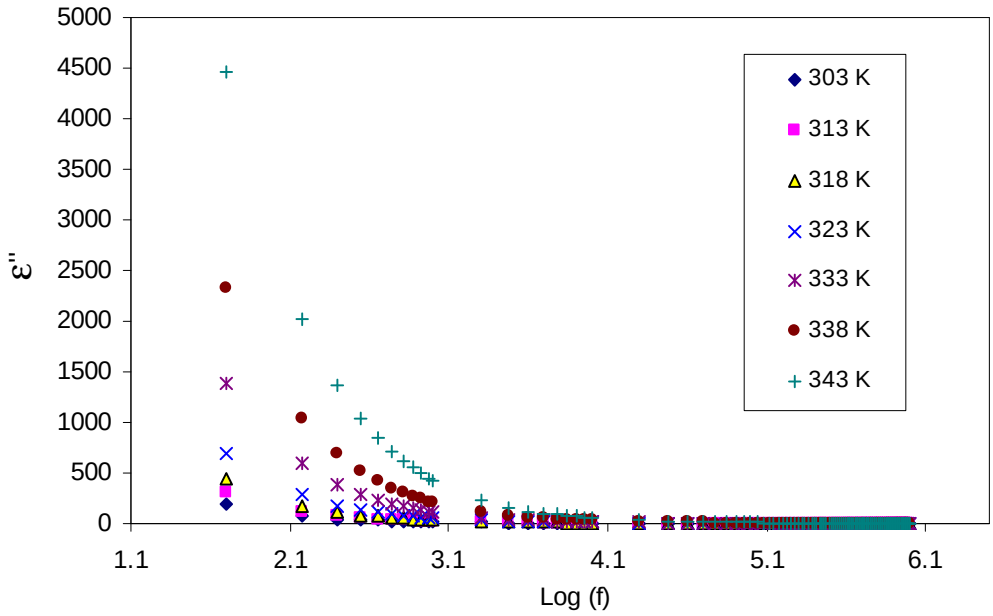

Figure 5.30 Frequency dependence of dielectric loss at different temperatures for CSB6 sample.

5.3.2 Frequency dependence of tan δ for CS:NaTf (CSB6) SPE

To obtain knowledge of the relaxation processes, i.e., whether the relaxation processes are Debye or non-Debye type, tan δ as a function of frequency at different temperatures for chitosan-sodium triflate (CSB6) membrane was plotted as shown in figure 5.31. It can be observed that tan δ increases with frequency, passes through a maximum value and thereafter decreases. It is clear from the figure that loss tangent maximum shift to higher frequency as the temperature increases. Shifting of the peak frequencies in the forward direction with temperature implies that as temperature increases, the relaxation time decreases. The broadness of the loss tangent peak indicates that the relaxation process

is non-Debye relaxation. The increase in height of tan δ with temperature could be attributed to the decrease in resistivity of the sample (Idris et al., 2007).

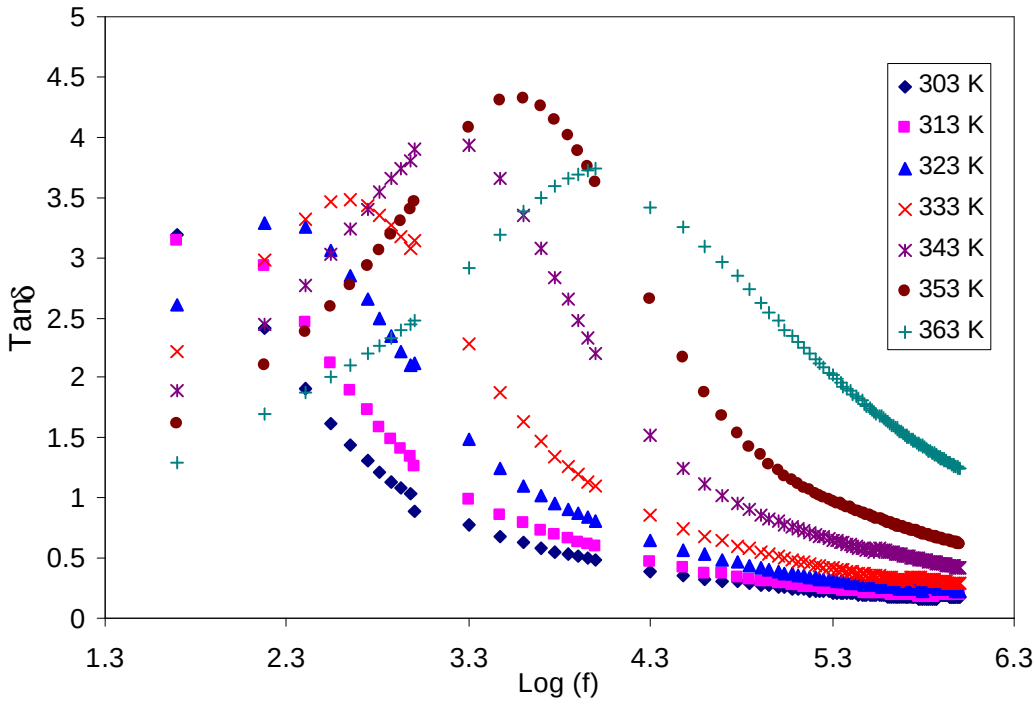

Figure 5.31 frequency dependence of loss tangent (tanδ) for CS:NaTf (CSB6) sample at different temperatures.

The reciprocal temperature variation of log (f_{max}) is shown in figure 5.32. The frequency-temperature relationship satisfies the Arrhenius behavior with the activation energy, E_a = 0.966 eV. The regression value R^2 is 0.983 indicating that all points lie on almost the same straight line. For this system the activation energy also is very close to that obtained from

plots of Log (σ) against 1000/T (1.2 eV). This is due to the fact that the ions participating in the conduction process are the same ions that relax.

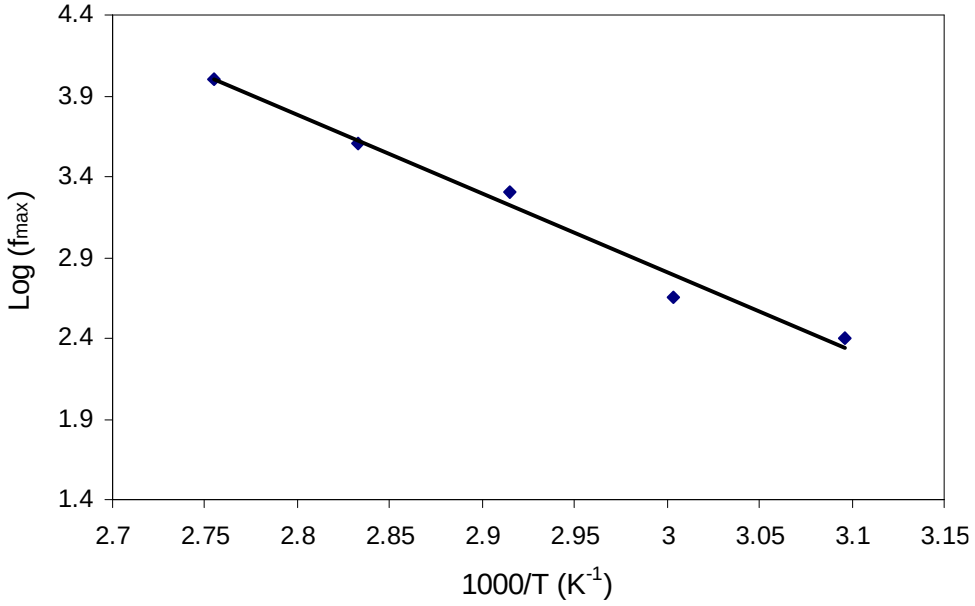

Figure 5.32 Temperature dependence of relaxation frequency for CSB6 sample.

5.3.3 Electric Modulus analysis of CSB6 system: Relaxation processes

A further analysis of the dielectric behavior could be more successfully achieved using electrical modulus formalism. Figure 5.33 shows the frequency dependence of real part (M') of complex modulus (M^*) at several temperatures for chitosan-sodium triflate (90:10) membrane. It can be seen that the real part of electric modulus (M') shows a small value in the low frequency region and large value at the high frequency end. It can be noticed that M' decreases with increase in temperature; this is opposite to that of

permittivity. This could be ascribed to the increase of conductivity with increasing temperature.

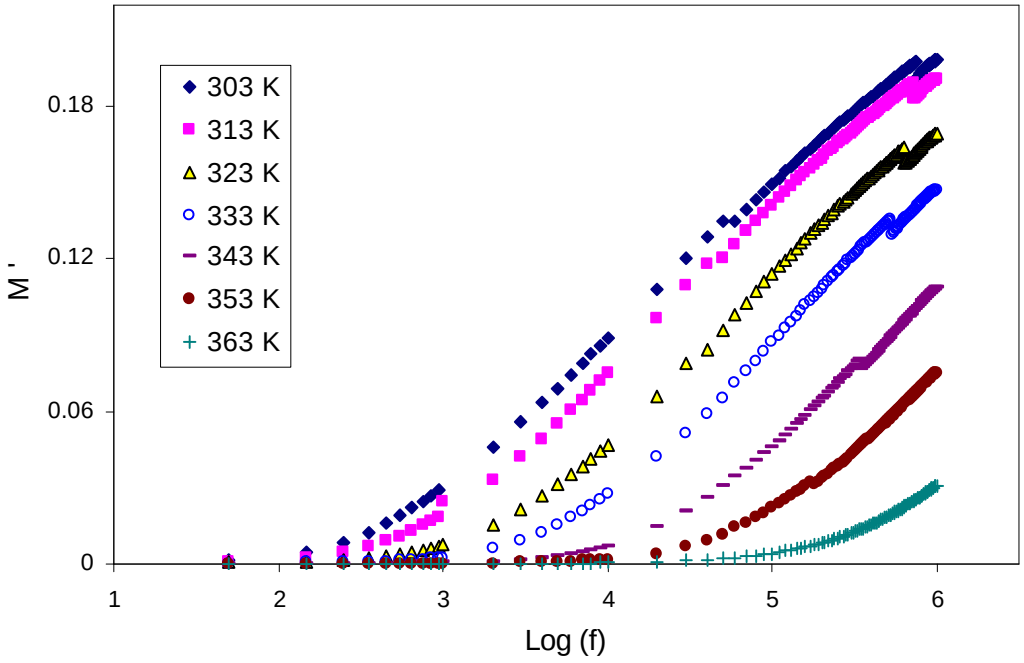

Figure 3.33 Frequency dependence of M′ at different temperatures for CSB6 sample.

The variation of *M''* with frequency for chitosan-salt (CSB6) system is shown in Fig. 5.34 at selected temperatures. At lower frequencies *M''* exhibits low value, which might be due to the large value of capacitance associated with the electrode/electrolyte polarization [Patro and Hariharan, 2009b]; however, at high frequencies a well-defined peaks are observed which indicate that the samples are ionic conductors. It can be seen that with increasing temperature the peaks shift to higher frequency which indicate the decrease of relaxation time for ion conduction.

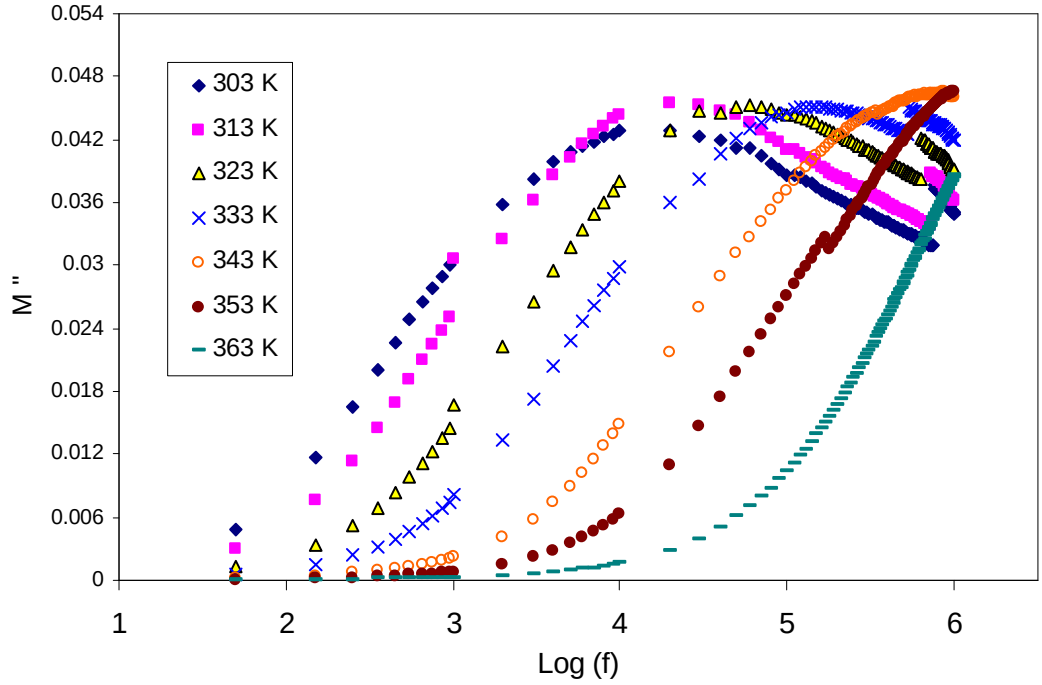

Figure 5.34 Frequency dependence of *M''* at different temperatures for CSB6 sample.

Fig. 5.35 shows the temperature dependence of Argand plots. It can be seen that the curves of Argand plot are incomplete semicircles which cannot be explained by Debye model (single relaxation time). In addition to ionic polarization in polymer electrolytes dipolar polarization and interfacial polarization are also in existence. These different polarization mechanisms results in a non-Debye behavior and thus the distribution of relaxation times. It can be observed that with increasing temperature the Argand curves shift towards the origin as occurred for CS:AgTf. This is again ascribed to the increase of conductivity resulting in increase of ionic mobility with temperature and thus the decrease of both Z_r and Z_i.

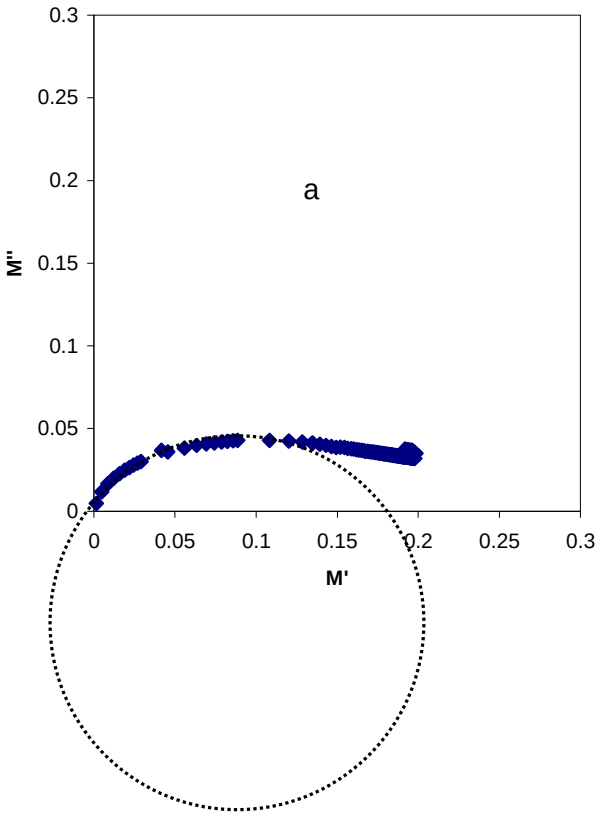
a
M''
M'
0.3
0.25
0.2
0.15
0.1
0.05
0
0
0.05
0.1
0.15
0.2
0.25
0.3

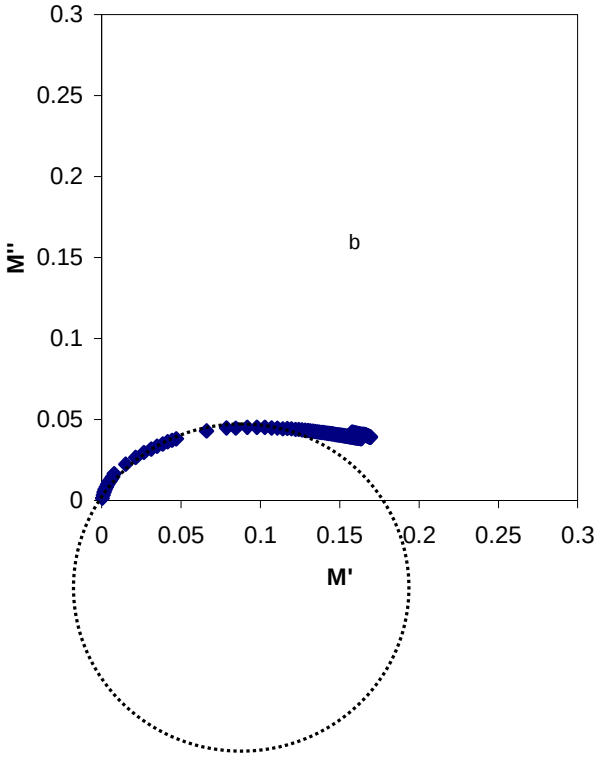
b
M''
M'
0.3
0.25
0.2
0.15
0.1
0.05
0
0
0.05
0.1
0.15
0.2
0.25
0.3

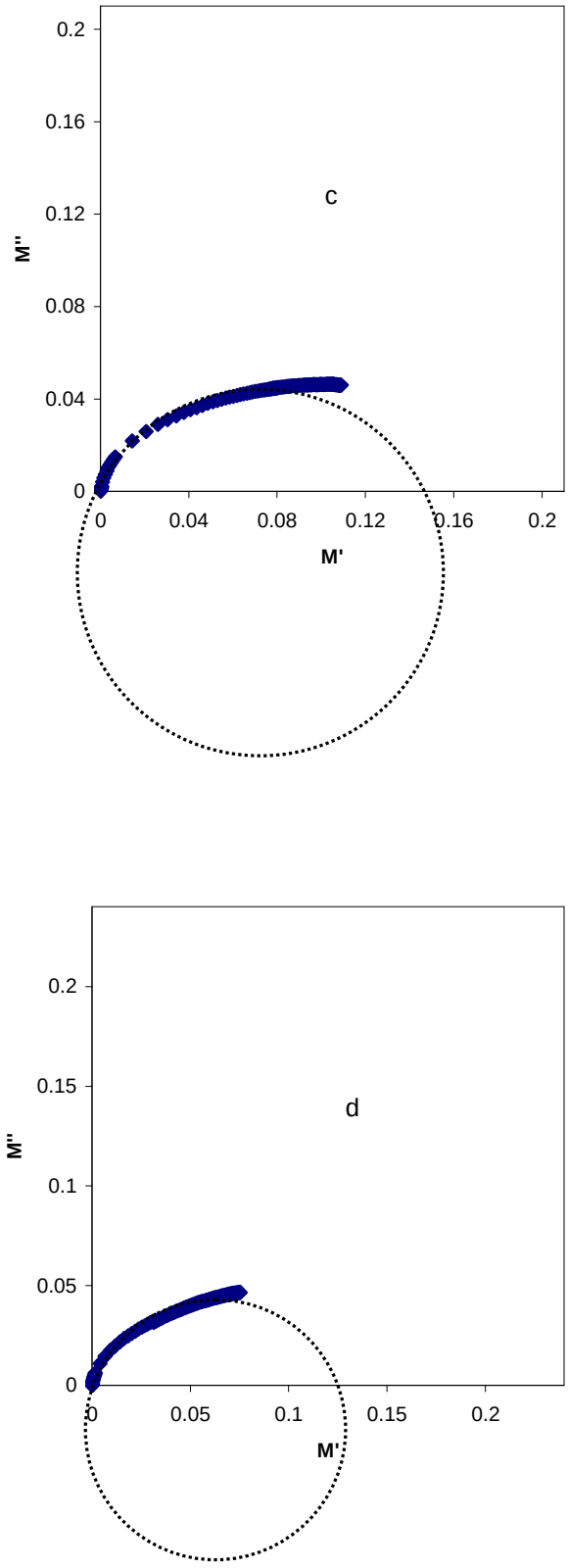

Figure 5.35 Argand plots for CS:NaTf (CSB6) at (a) 303 K, (b) 323 K, (c) 333 K and (d) 343 K.

5.3.4 Correlation between impedance and AC conductivity (σ_{ac}) of SPE based on CS:NaTf (CSB6)

Electrical impedance plots (Z_i vs Z_r) for CSB6 are shown in Fig. 5.36(a-e) at different temperatures. It can be seen that the plots show two obvious regions, i.e., a high frequency semicircle region which is due to the bulk effect of the solid electrolyte and a low frequency spike region that is ascribed to the effect of blocking electrodes and known as electrode polarization (EP). It is clear that the high frequency semicircle diameter gradually decreases with increase in temperature and almost disappears at 413 K. The disappearance of the high frequency semicircular region in the impedance plot at higher temperatures led to an inference that the total conductivity is mainly due to the result of ion migration and thus a large amount of charge carriers can be accumulated at the electrode/electrolyte interface (EP effect) [Rajendran et al., 2008].

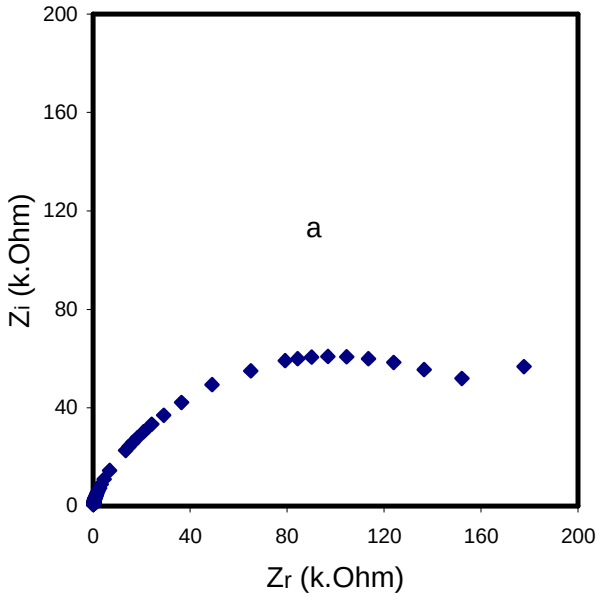

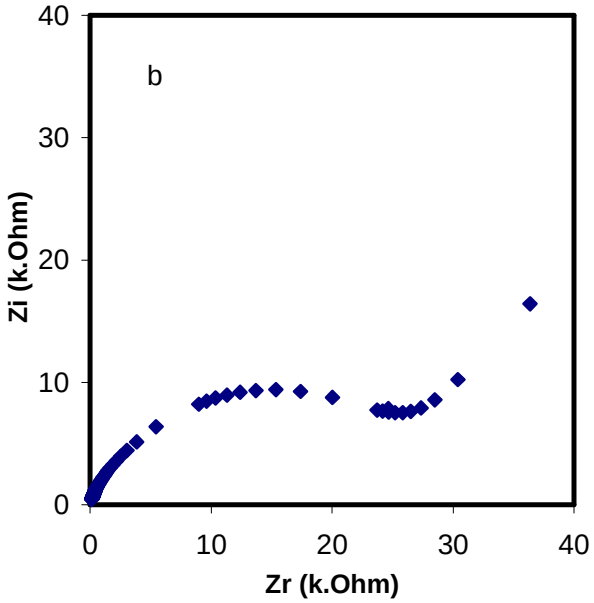
b
Zi (k.Ohm)
Zr (k.Ohm)
0
10
20
30
40

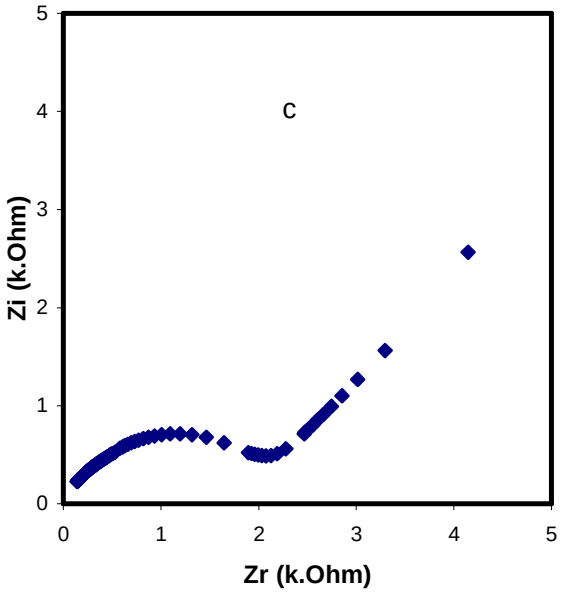
c
Zi (k.Ohm)
Zr (k.Ohm)
0
1
2
3
4
5

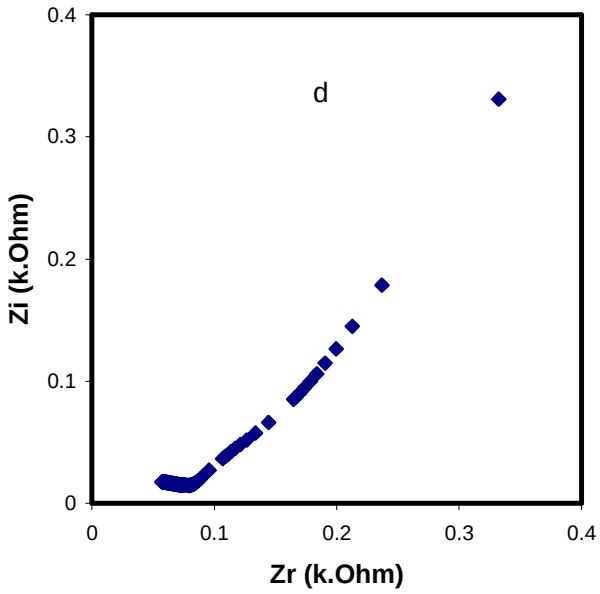

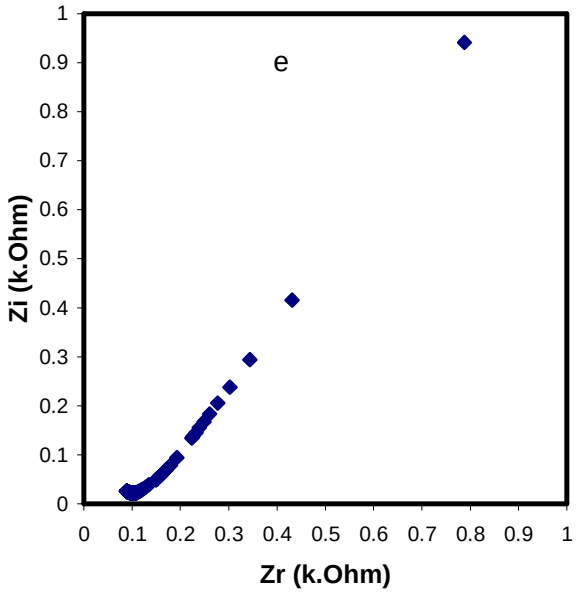

Figure 5.36 Impedance plots of chitosan:$NaCF_3SO_3$ (CSB6) at (a) 313 K, (b) 333 K, (c) 353 K, (d) 373 K and (e) 413 K.

AC conductivity as a function of frequency at different temperatures is shown in Fig 5.37 (a-f) for chitosan-$NaCF_3SO_3$ (CSB6). The ac conductivity spectra from Fig 5.37 (a) to 5.37 (d) can be divided into three distinct regions. The low frequency region (I) which appeared as a spike is due to electrode-electrolyte interfacial phenomena, i.e., electrode polarization [Hema et al., 2008]. It can be noticed that the contribution of the spike region (I) in Fig. 5.37 (a-f), increases with an increase in temperature. These regions (region I, Fig. 5.37)) exhibits similar behavior with temperature as occurred in impedance plots (spike regions). In the intermediate frequency region (II) a plateau-like ac conductivity is observed. This corresponds to DC conductivity which decreases significantly with increasing temperature as a result of electrode polarization enhancement and shifts to the higher frequency side. In the high frequency region (III) the ac conductivity increases with increasing frequency and shows the power law dispersion. At higher temperatures the dispersion regions disappear as a result of dominant electrode polarization. These results are strongly supported by impedance plots (Fig. 5.36 (e-d)) at high temperatures where only spikes are exhibited.

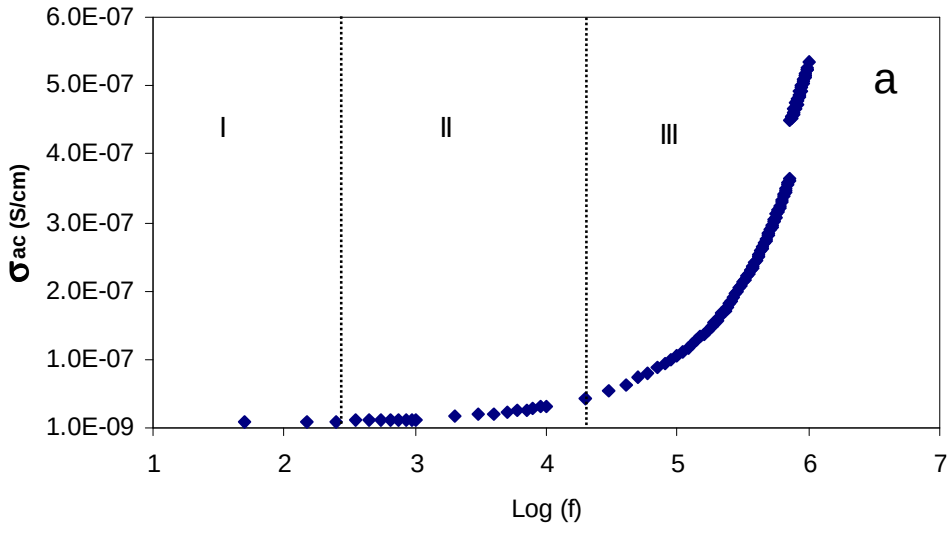

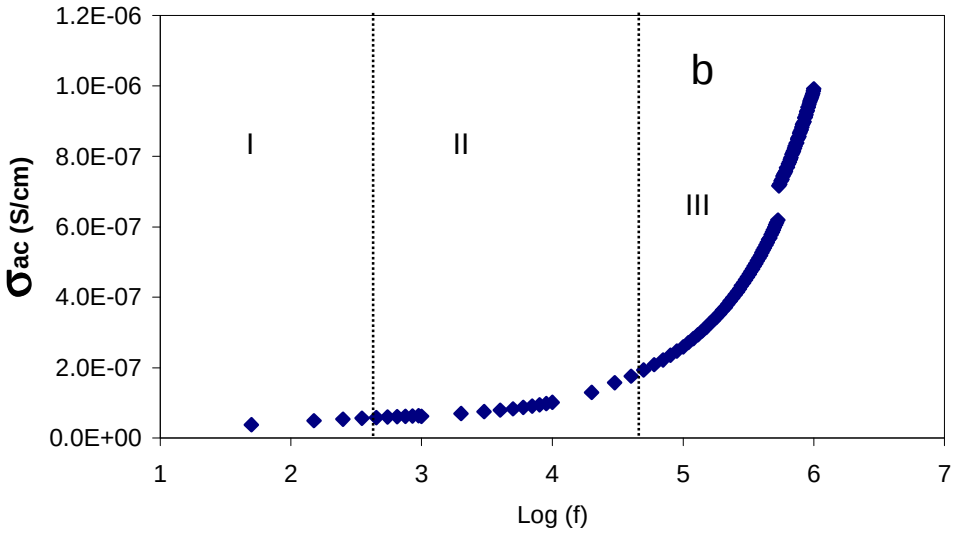
1.2E-06
1.0E-06
8.0E-07
6.0E-07
4.0E-07
2.0E-07
0.0E+00
σac (S/cm)
b
I
II
III
1
2
3
4
5
6
7
Log (f)

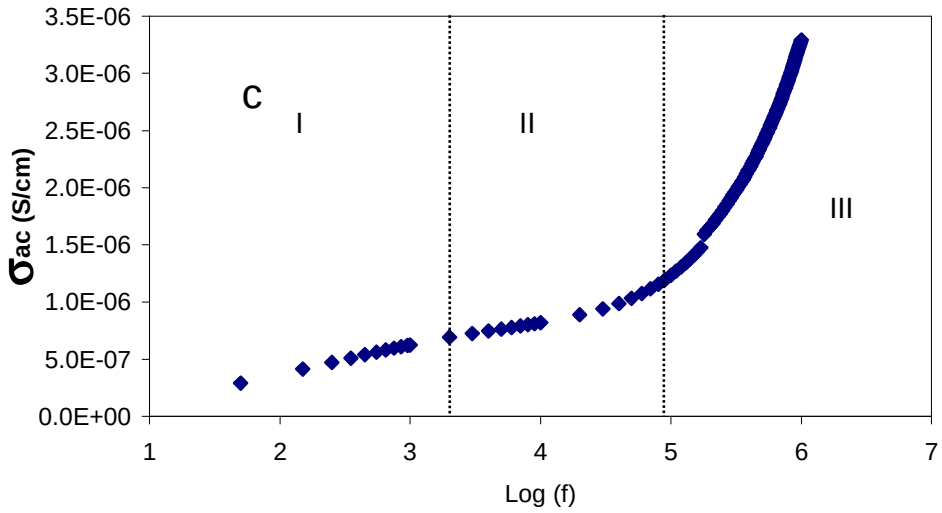
3.5E-06
3.0E-06
2.5E-06
2.0E-06
1.5E-06
1.0E-06
5.0E-07
0.0E+00
σac (S/cm)
c
I
II
III
1
2
3
4
5
6
7
Log (f)

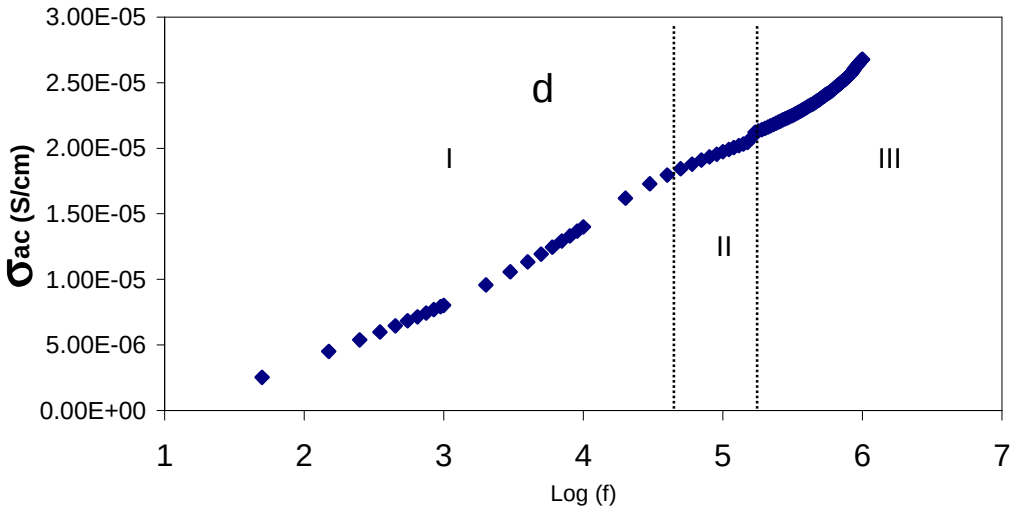
3.00E-05
2.50E-05
2.00E-05
1.50E-05
1.00E-05
5.00E-06
0.00E+00
σac (S/cm)
d
I
II
III
1
2
3
4
5
6
7
Log (f)

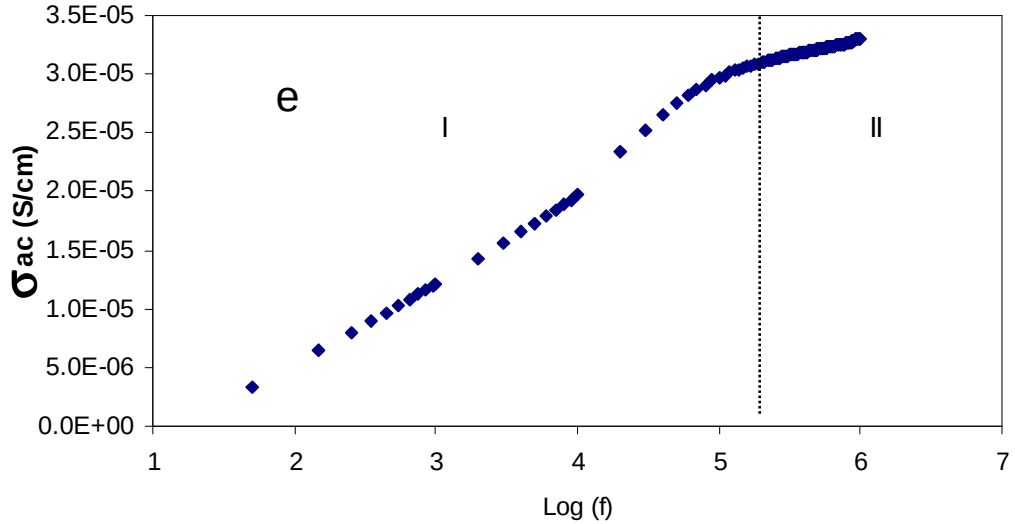
3.5E-05
3.0E-05
2.5E-05
2.0E-05
1.5E-05
1.0E-05
5.0E-06
0.0E+00
σac (S/cm)
e
I
II
1
2
3
4
5
6
7
Log (f)

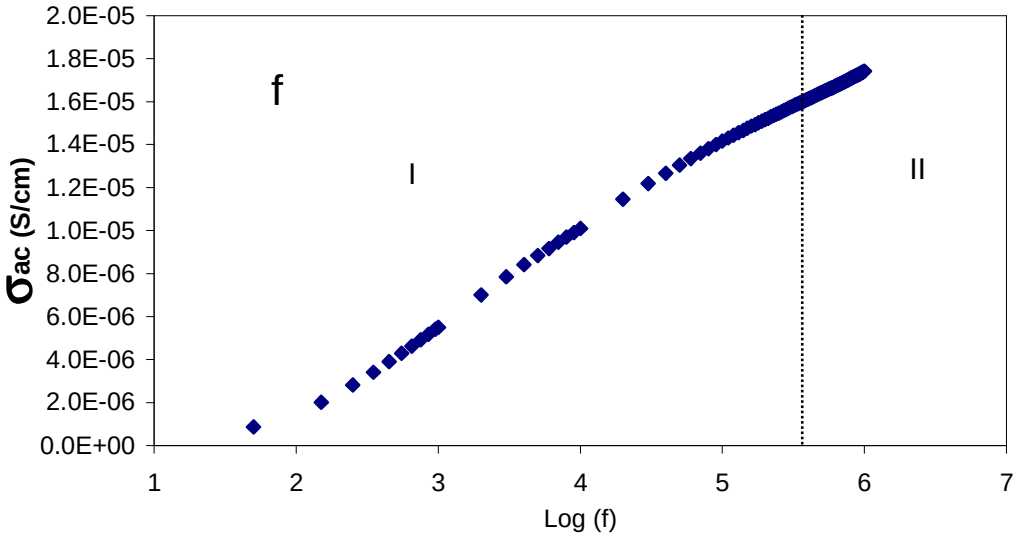

Figure 5.37 AC conductivity spectra of chitosan:$NaCF_3SO_3$ (CSB6) at (a) 313 K, (b) 333 K, (c) 353 K, (d) 373 K, (e) 393 K and (f) 413 K.

The value of the frequency exponent s is determined from the slope of log (σ_{ac}) versus log (ω) at the dispersion region to characterize the type of ion conduction in CS:NaTf solid polymer electrolytes. As shown in Fig.5.38, the s value is temperature dependent; and it was observed that the s value decreases with increasing temperature to a minimum value and then increases slightly above 393 K. In the overlapping-large polaron tunneling (QLPT) model [Faraga et al., 2010], the exponent s depends on both frequency and temperature and drops with rising temperature to a minimum value and then increases slightly, as temperature rises. Thus OLPT model is the most suitable model to characterize the electrical conduction mechanism in chitosan-$NaCF_3SO_3$ solid electrolytes in the low (I) and high temperature (II) regions.

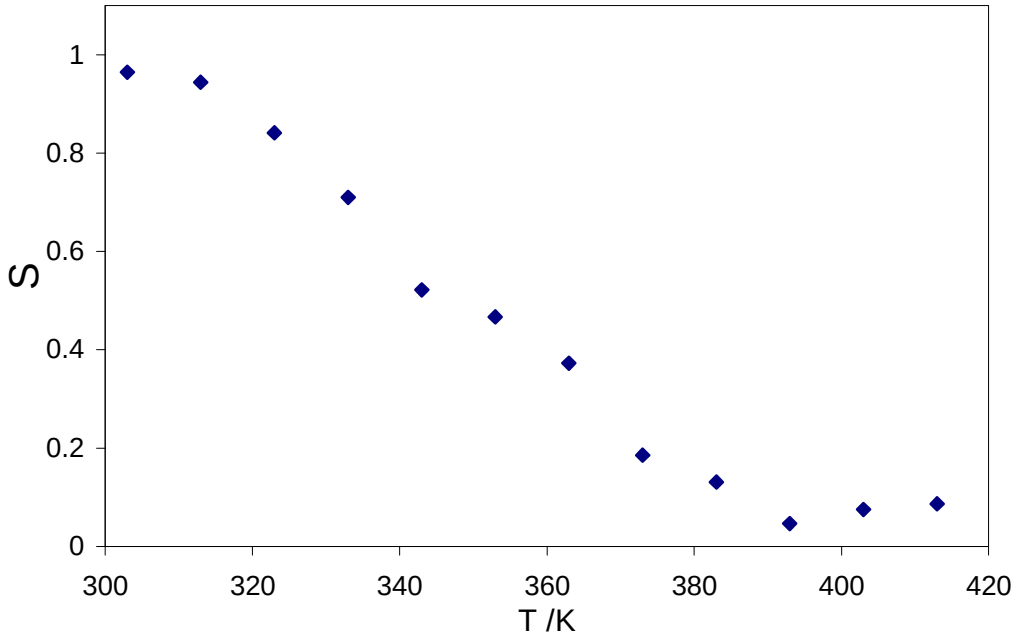

Figure 5.38 Temperature dependence of the frequency exponent s for CSB6 sample.

5.4 Electrical/Dielectric properties of SPEs based on CS:LiTf

5.4.1 DC conductivity and Dielectric analysis of SPE based on CS:LiTf

Figure 5.39 shows the variation of DC conductivity with various concentration of $LiCF_3SO_3$. It can be noted that the room temperature DC ionic conductivity of the chitosan based electrolyte increases with increasing LiTf concentrations. The increase in DC conductivity can be attributable to the increase in charge carrier density.

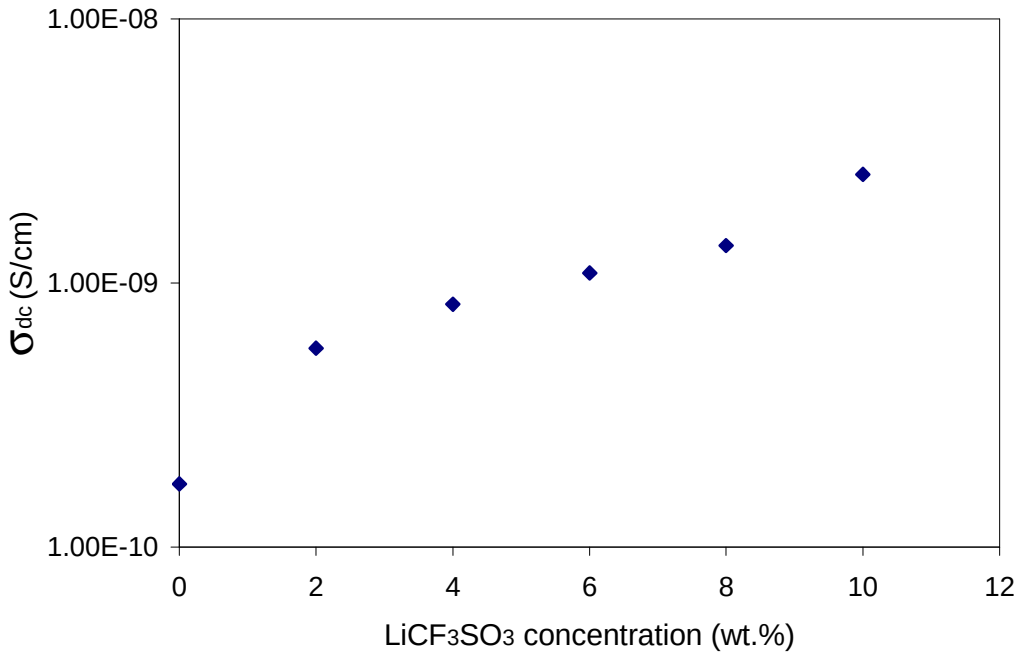

Figure 5.39 DC conductivity as a function of $LiCF_3SO_3$ concentration.

Figure 5.40 shows the variation of DC conductivity with reciprocal temperature for different salt concentrations. It is obvious that the DC conductivity increases almost linearly with rise in temperature in the low temperature region (region I) and is very similar to the CS:NaTf system. The linear relations which are observed in all chitosan: $LiCF_3SO_3$ compositions in region I again indicate that there is no phase transition in the polymer electrolyte [Selvasekarapandian et al., 2005], i.e., the temperature dependence of ionic conductivity in the low temperature region is of the Arrhenius type as occurred for the other two systems. The calculated E_a value for the highest conducting sample is 1.28 eV. The

drop of dc conductivity at higher temperatures in region II is attributed to the desorption of water.

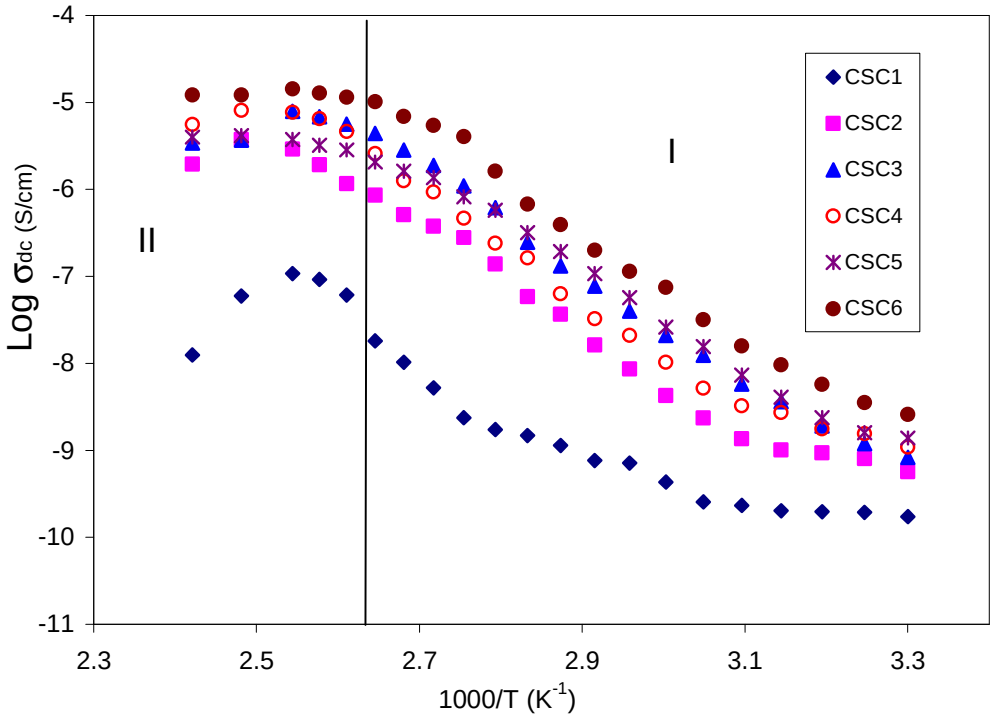

Figure 5.40 Temperature dependence of ionic conductivity for CS:LiTf SPEs.

Figure 5.41 shows the concentration dependence of dielectric constant at different frequencies. The low frequency region (I) shows the dispersion while the high frequency region (II) is almost constant which represent the materials property. It can be noticed that the chitosan:$LiCF_3SO_3$ (CSC6) sample i.e., the most amorphous sample exhibits higher dielectric constant compared to other samples. The increase in dielectric constant means an increase in charge carrier concentration.

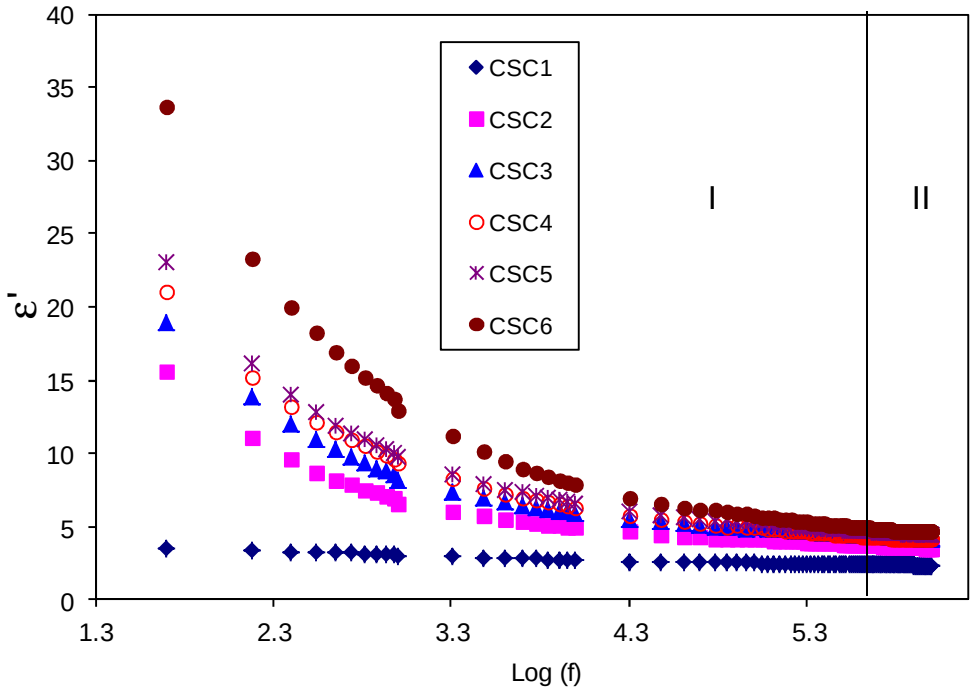

Figure 5.41 Compositional dependence of dielectric constant for CS:LiTf SPEs.

Figure 5.42 shows the composition dependence of bulk dielectric constant (high frequency region, II). It can be seen that the high conducting sample exhibits high dielectric constant. This can be ascribed to the high charge carrier concentration. When salt dissociates into polymer matrix, it forms mobile cations and anions. Under the influence of an electric field, ions tend to move along the field appropriately. However, movable charge carriers are unable to cross the blocking electrode-electrolyte interface

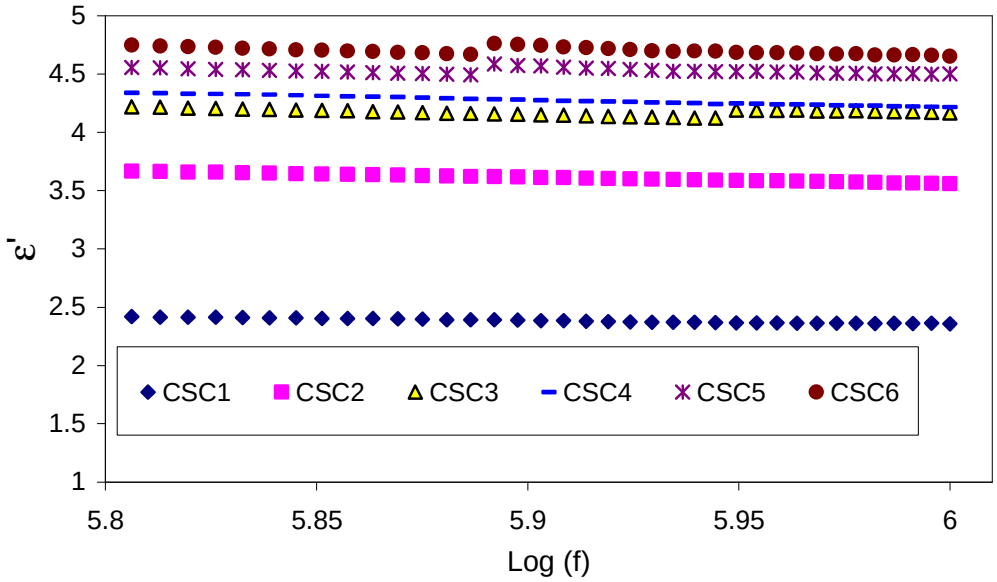

Figure 5.42 Compositional dependence of bulk dielectric constant for CS:LiTf SPEs.

Figure 5.43 shows the concentration dependence of bulk dielectric constant and DC conductivity. The behavior of dielectric constant and DC conductivity with LiTf salt is the same.

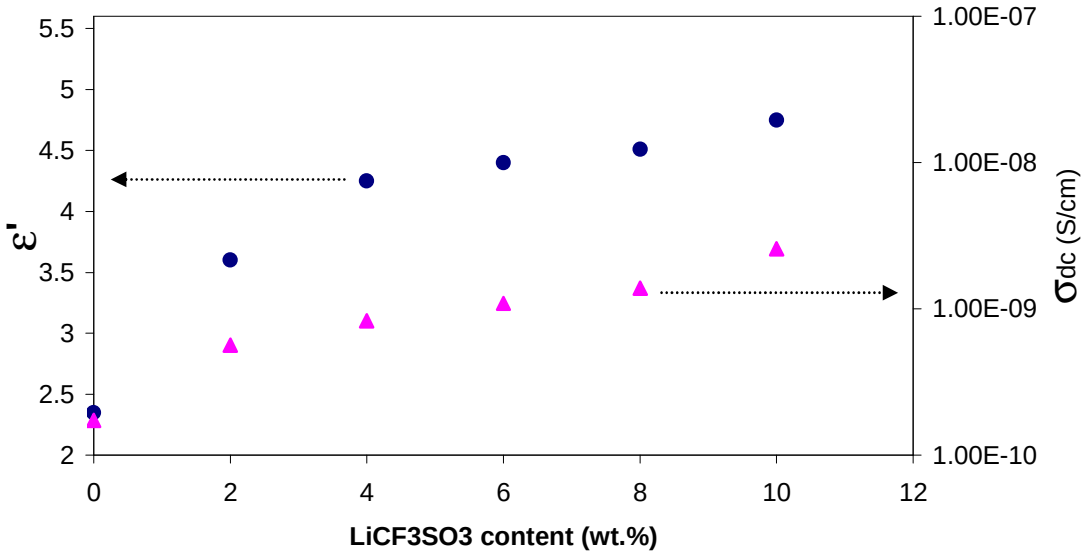

Figure 5.43 Variation of dielectric constant and DC conductivity with various LiTf concentrations.

Figure 5.44 shows the variation of dielectric constant with frequency at different temperatures for chitosan-$LiCF_3SO_3$ (CSC6). It is obvious that the dielectric constant shows the high value at low frequency due to electrode polarization effect. The high frequency region which appeared as a plateau is related to the bulk property of the sample is also temperature dependent as depicted in Fig 5.45. The increase in bulk dielectric constant with increasing temperature indicates the increase in charge carrier concentration because dielectric constant represents the storage of charge carriers. This is can be explained on the fact that in polar polymers, ε′ increases with temperature. Because, temperature can facilitates the orientation of dipoles and this result in increased permittivity [Bhargav, et al., 2009]. The increase in permittivity leads to dissociation of more ions that are able to participate in polarization as well as in conduction. Thus the increase of bulk dielectric constant means an increase of bulk DC conductivity because both are calculated from the high frequency semicircle. The results of CS:LiTf together with CS:AgTf and CS:NaTf systems demonstrate a strong correlation between DC conductivity and dielectric constant.

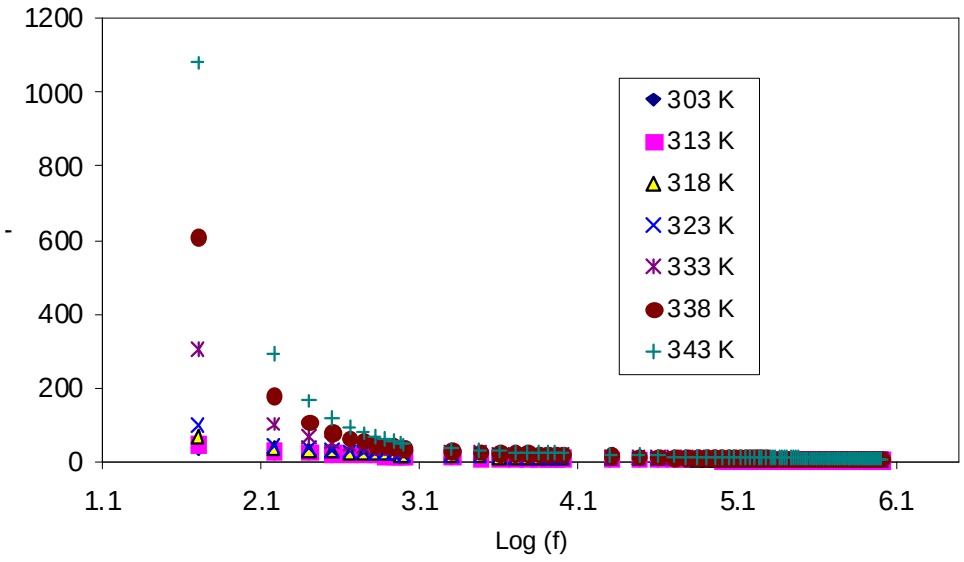

Figure 5.44 Frequency dependence of dielectric constant (ε′) for CSC6, at different temperatures.

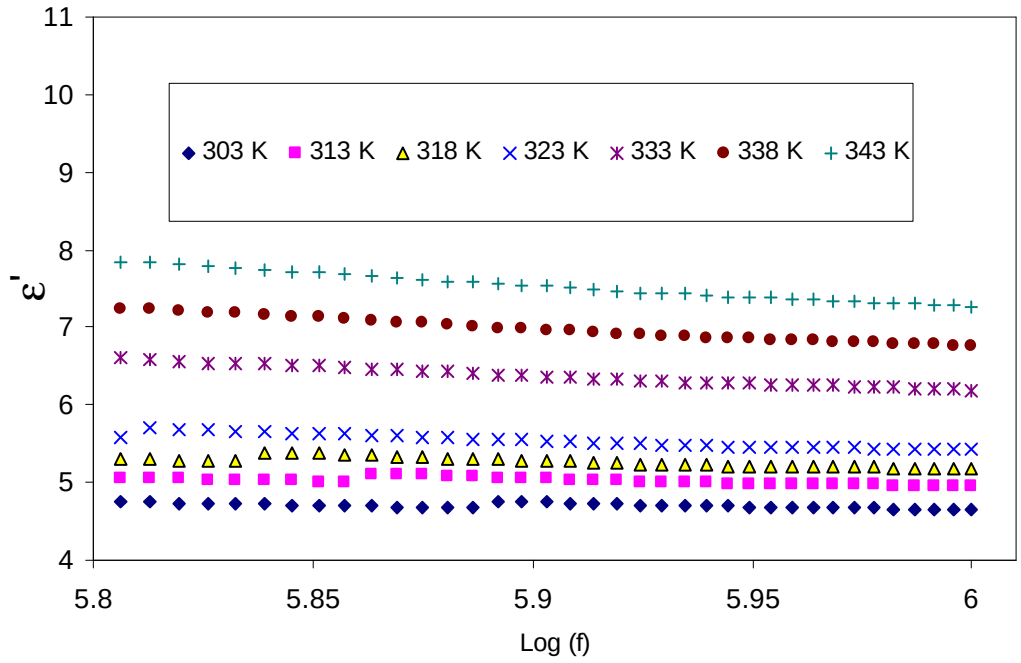

Figure 5.45 Frequency dependence of bulk dielectric constant (ε′) for CSC6 sample, at different temperatures.

Figure 5.46 shows the smooth curve between DC conductivity and dielectric constant at different temperatures. This result reveals that an increase in dielectric constant means an increase in charge carrier concentration and consequently an increase in DC conductivity ($\sigma = \Sigma qn\mu$). This smooth curve is similar to that obtained for CS:AgTf (CSA6) and CS:NaTf (CSB6) systems. Thus similar trends of bulk DC conductivity and bulk dielectric constant with slat concentration in CS:AgTf, CS:NaTf and CS:LiTf solid polymer electrolytes and the smooth curve between DC conductivity and dielectric constants confirm the strong relationship between DC and dielectric constant . Thus the study of dielectric constant is powerful method to study the conductivity behavior of

polymer electrolytes. One point of conductivity can be selected on this curve as a reference to scale the DC conductivity.

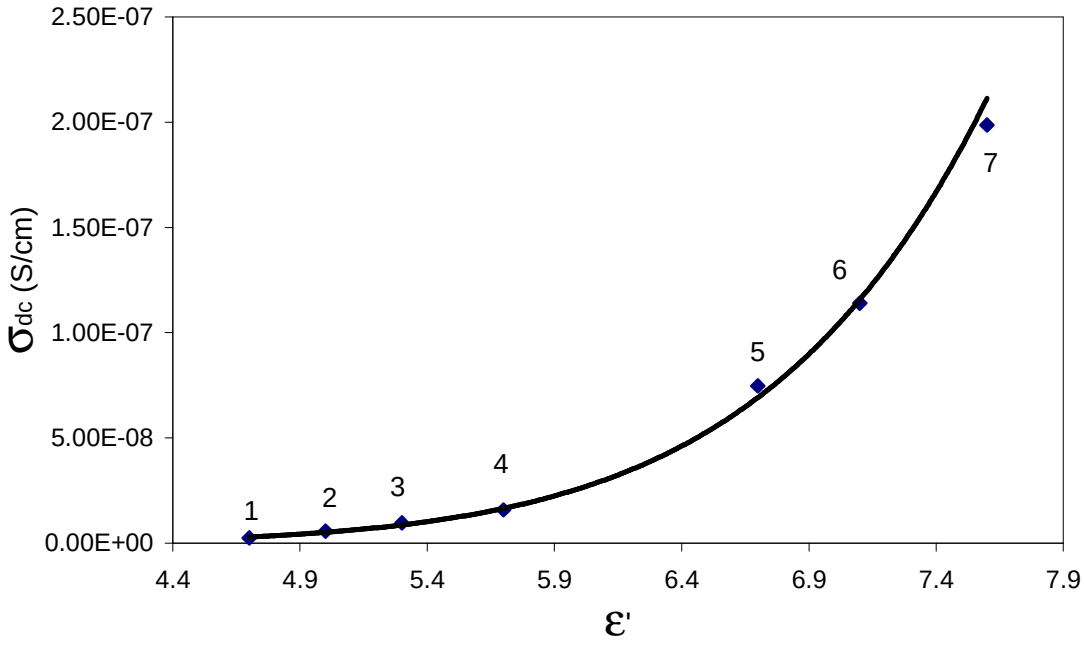

Figure 5.46 DC conductivity dependence on dielectric constant at, (1) 303, (2) 313, (3) 318, (4) 323, (5) 333, (6) 338 and (7) 343 K for CSC6 sample.

Figure 5.47 demonstrates the compensated Arrhenius behavior for the temperature dependence of conductivity for CSC6 complex system scaled at a reference temperature of 333 K. It can be seen that there is no distinguishable difference between the temperature dependence of compensated Arrhenius and normal Arrhenius relation exhibited in Fig 5.40. The slope gives an activation energy of 1.27eV which is very close to the calculated one from normal Arrhenius relation. The calculated activation energy from the compensated Arrhenius plot was used to evaluate the pre-exponential factor (σ_o).

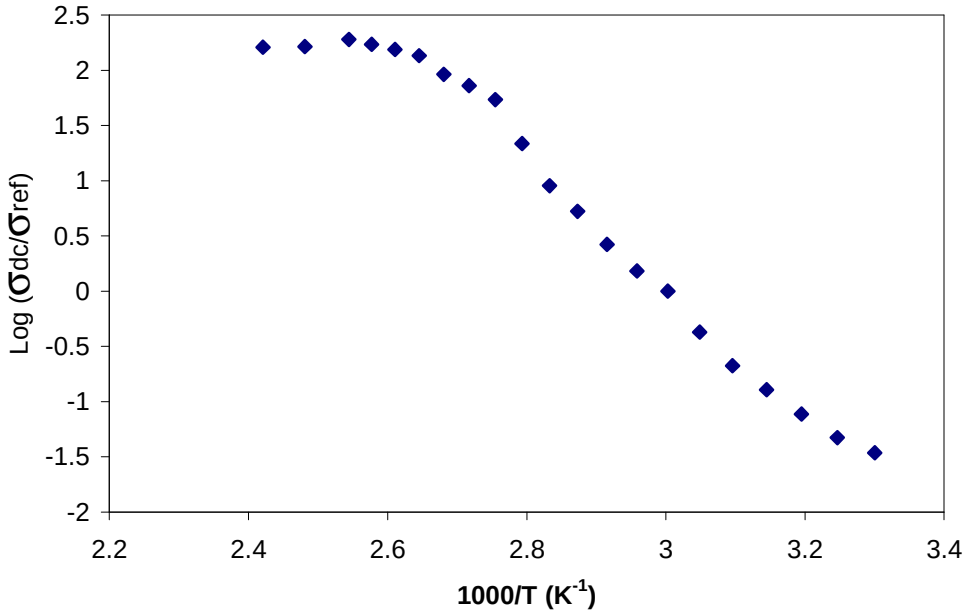

Figure 5.47 Compensated Arrhenius equation plotted against the reciprocal temperature for CSC6 system.

The results of Fig 5.48 demonstrates the temperature and dielectric constant independent of pre-exponential factor for CS:LiTf solid electrolyte which is almost the same to that obtained for CS:AgTf and very similar to CS:NaTf system. Thus the results of CS:LiTf solid electrolyte is also do not follows the Petrowsky and Frech work [2009, 2010], which gives a smooth curve between pre-exponential factor and dielectric constant. Thus, these results of the three studied solid electrolytes confirms the applicability and satisfactory of normal Arrhenius relation in solid polymer electrolytes and reveals the constant behavior of pre-exponential factor. The non existence of distinguishable differences between compensated Arrhenius and normal Arrhenius is also indicative that Petrowsky and Frech hypothesis is not applicable for chitosan based solid electrolyte.

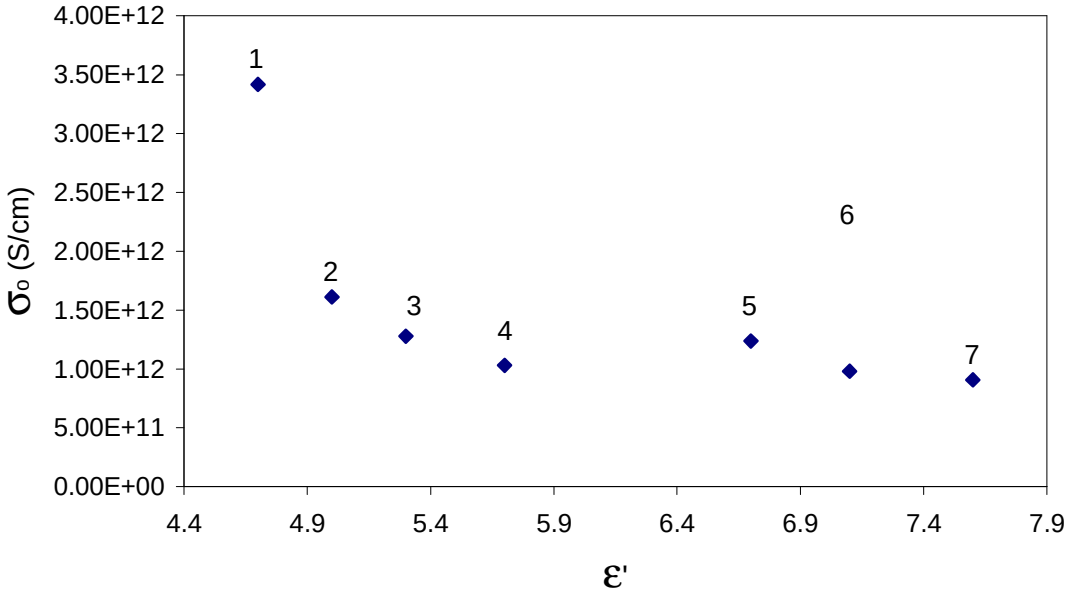

Figure 5.48 Temperature and dielectric constant dependent of pre-exponential factor (σ_o) at (1)303, (2) 313, (3) 318, (4) 323, (5) 333, (6) 338 and (7) 343 K for CSC6 system.

Figure 5.49 shows the frequency dependence of dielectric loss for CSC6.

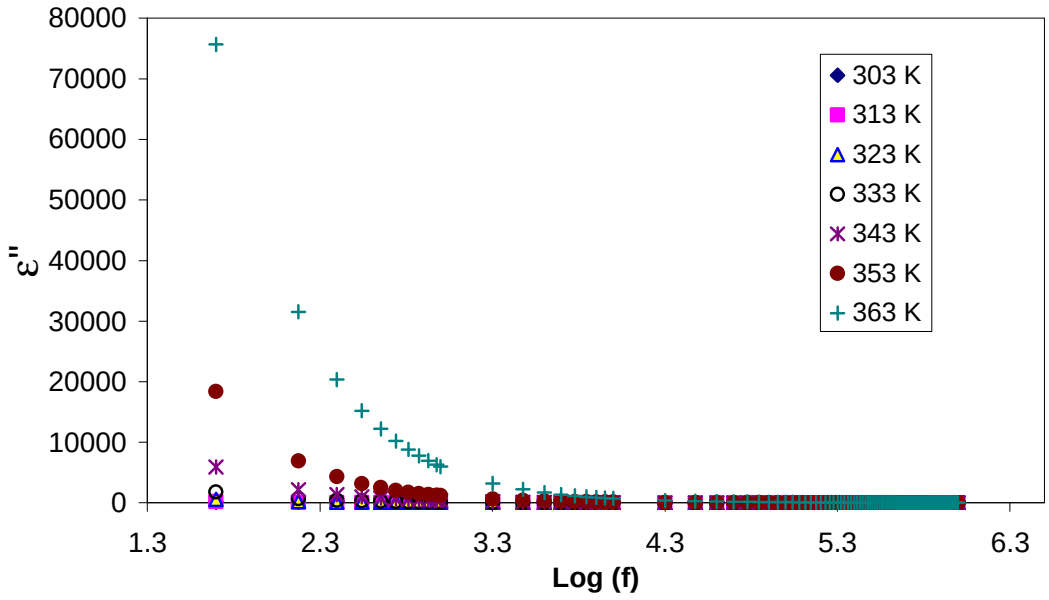

Figure 5.49 Frequency dependence of ε″ at selected temperatures for CSC6 sample.

It can be seen (Fig. 5.49) that the dielectric loss spectra show dispersion at low frequencies and are almost constant at high frequency. At low frequencies, due to the long period and thus show reversal of the electrical field, the mobile ions tend to accumulate at the electrode/electrolyte interface. This gives a high value of dielectric loss (ε″). The high value of dielectric loss compare to dielectric constant can be attributable to DC contribution to loss spectra. This behavior is similar to the other two systems.

5.4.2 Frequency dependence of Tan δ of SPE based on CS:LiTf (CSC6)

Figure 5.50 shows tan δ as a function of frequency at different temperatures for chitosan-lithium triflate (CSC6) sample.

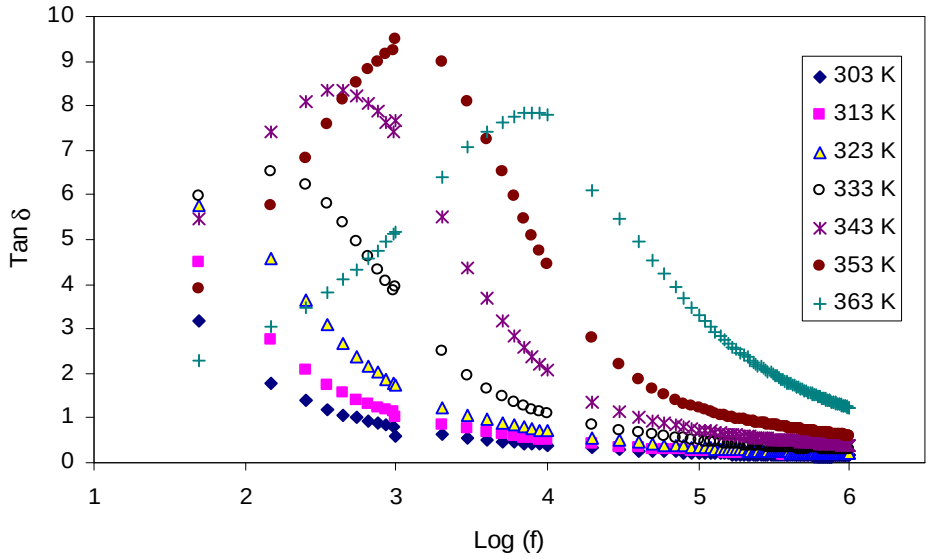

Figure 5.50 Frequency dependence of tanδ at different temperatures for CSC6 system.

It can be observed that tan δ increases with frequency, passes through a maximum value and thereafter decreases. It can be seen that the loss tangent maximum shifts to higher

frequency as the temperature increases, indicating that the relaxation time decreases and the conductivity increases, i.e., the resistivity of the sample decreases. The broadness of the peaks indicates the non-Debye behavior of the relaxation processes.

The frequency-temperature relationship as depicted in Fig 5.51 satisfies the Arrhenius behavior with the activation energy, E_a = 1.25 eV. The regression value R^2 is 0.986 indicating that all points lie on almost the same straight line.

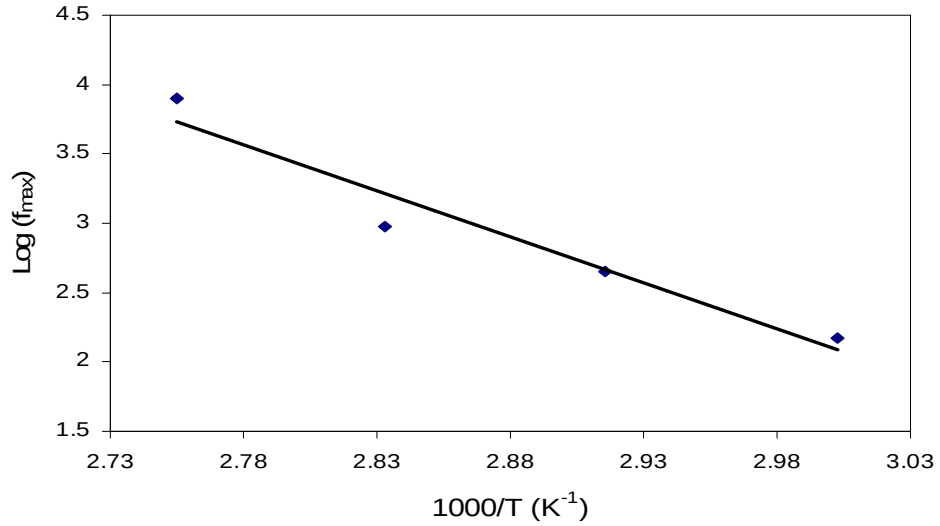

Figure 5.51 Temperature dependence of relaxation frequency for CSC6 sample.

5.4.3 Electric Modulus Analysis of CSC6 system: Relaxation processes

Figure 5.52 shows the frequency dependence of the real part M′ of electric modulus at different temperatures for the sample with the highest dielectric constant and DC

conductivity (CSC6). The long tail at low frequency is attributed to the high capacitance associated with the electrodes (EP effect). The decrease of M′ is due to the increase of dielectric constant at higher temperatures. In other words the decrease of M′ with increasing temperature can be ascribed to the increase of carrier density and decrease of resistance.

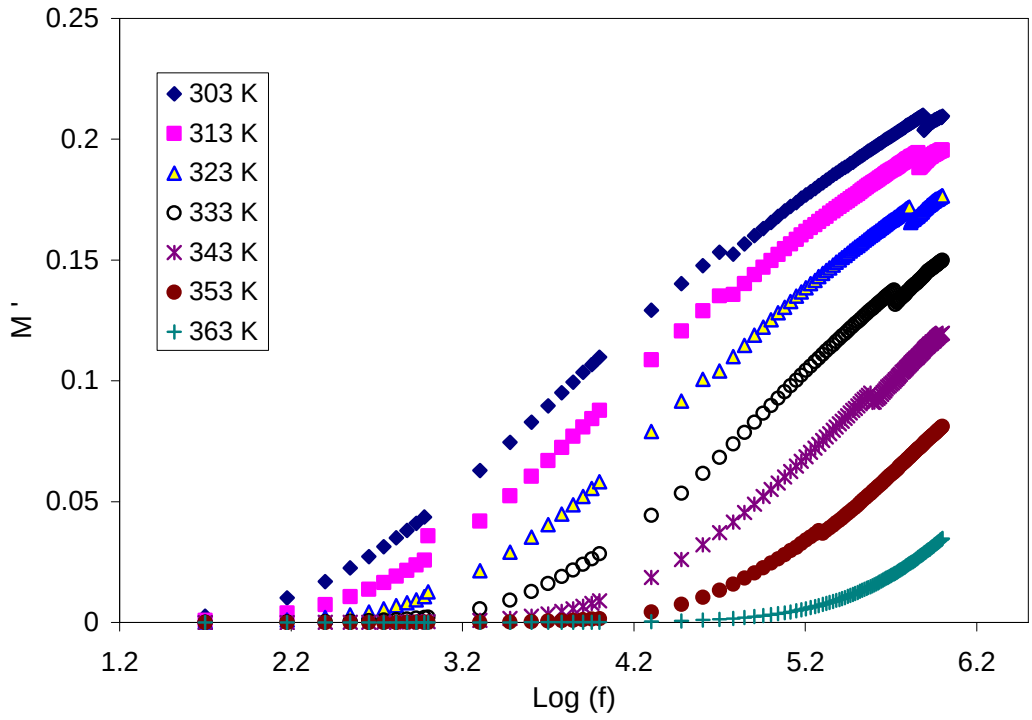

Figure 5.52 Frequency dependence real part (M′) of M* for chitosan:$LiCF_3SO_3$ (CSC6) at different temperature.

Figure 5.53 shows the imaginary part of electric modulus as a function of frequency at different temperatures for the CSC6 sample. The M″ spectra exhibit an obvious relaxation peak. This suggests an ionic motion contributes to DC conductivity obscures the relaxation

peaks in ε″ spectra [Sengwa et al., 2008b]. Shifting of the maximum peak frequency M″ spectra in the forward direction with temperature implies that as the temperature is increased, the conductivity relaxation time decreases.

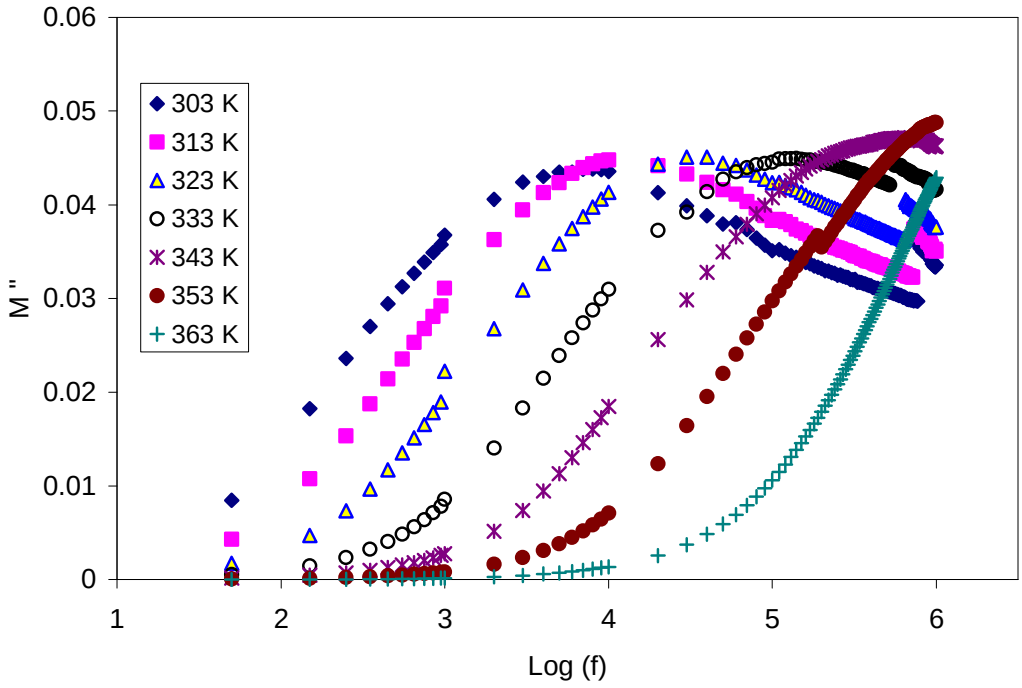

Figure 5.53 Frequency dependence imaginary part (M″) of M* for chitosan $LiCF_3SO_3$ (CSC6) at different temperature.

Fig. 5.54 shows the Argand plots for CSC6 sample at selected temperatures. It can be seen that the Argand plot consists of an incomplete half semicircle like CS:AgTf and CS:NaTf systems. Thus the relaxation processes cannot be explained by Debye model (non-interacting or ideal dipoles). The Debye relaxation is the dielectric relaxation response of an ideal, non-interacting population of dipoles to an alternating external electric field [Hill and Dissado, 1985]. For a pure monodispersive Debye process, one expects semicircular plots

with a center located on the real axis in Argand plots whereas, for distributive relaxation, these Argand plane plots are close to circular arcs with a center below the real axis [Dutta and Sinha, 2006]. The non-Debye behavior can be ascribed to the distribution of relaxation time over a range of frequencies due to the contribution of different polarization mechanisms such as ionic, dipolar, and interfacial polarization. The broadness and asymmetric nature of Argand plots reveal the distribution of relaxation time. The shifting of the curves towards the origin with increasing temperature can be attributed to the decrease of resistivity which can be easily deduced from the equations of M′ and M″.

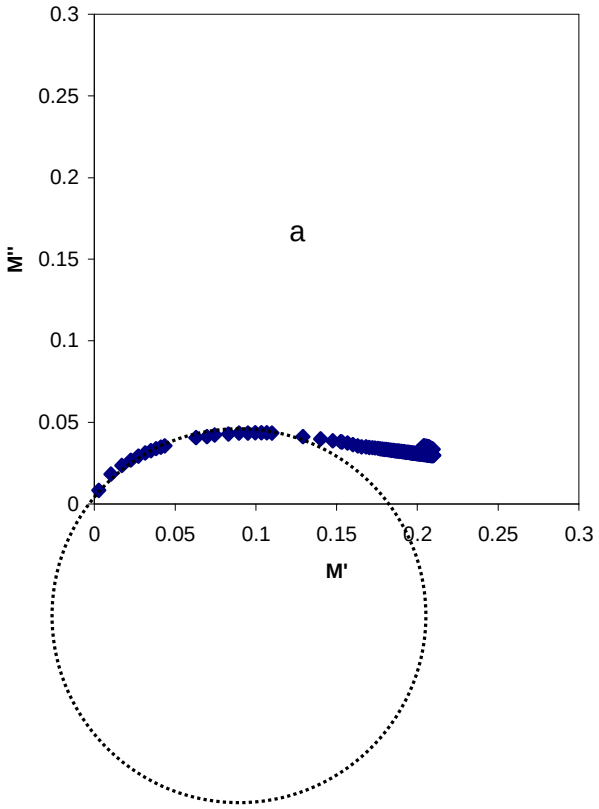

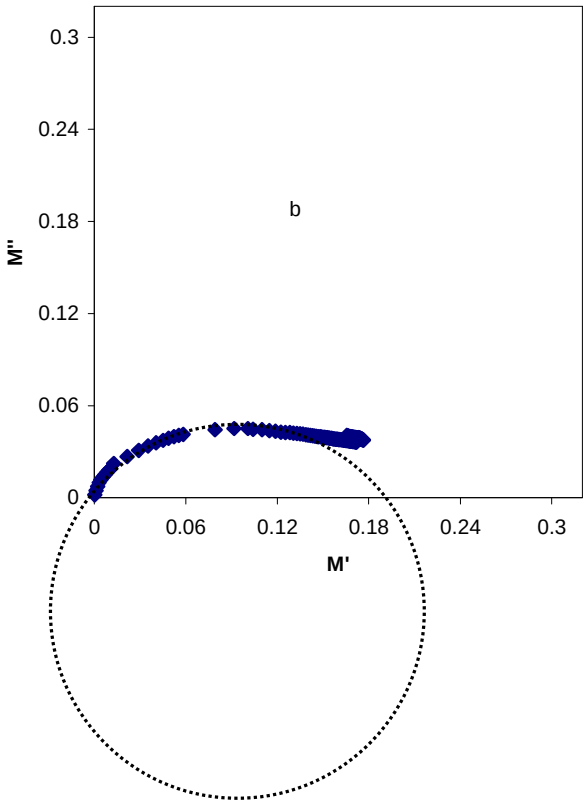
b
M''
M'
0.3
0.24
0.18
0.12
0.06
0
0
0.06
0.12
0.18
0.24
0.3

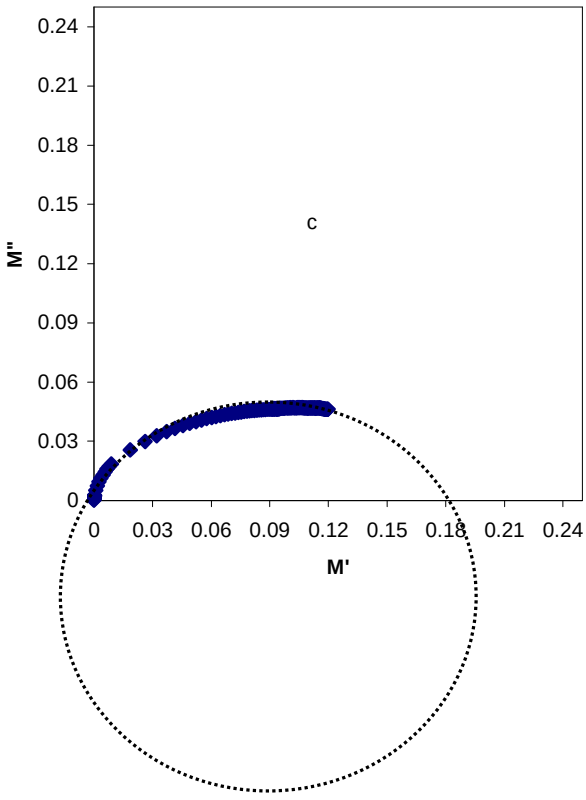
c
M''
M'
0.24
0.21
0.18
0.15
0.12
0.09
0.06
0.03
0
0
0.03
0.06
0.09
0.12
0.15
0.18
0.21
0.24

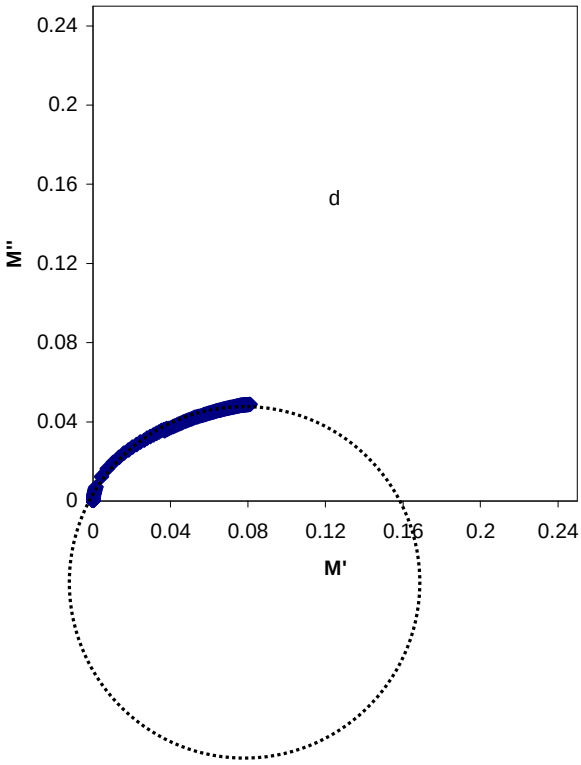

Figure 5.54 Argand plots for chitosan:$LiCF_3SO_3$ (CSC6) at (CSA6) at (a) 303 K, (b) 323 K, (c) 333 K and (d) 343 K

5.4.4 Correlation between impedance and AC conductivity (σ_{ac}) of SPE based on CS:LiTf (CSC6)

Figure 5.55(a-e) shows the electrical impedance plots (Z_i vs Z_r) for CSC6 sample at different temperatures. The advantage of impedance plots is that the contribution of bulk (high frequency semicircle) and electrode polarization (low frequency spike) can be easily separated as depicted in Fig 5.55. The behavior of CS:LiTf system is similar to CS:NaTf system with temperature, i.e., with increase in temperature the diameter of the high

frequency semicircle is decreased and almost disappear at high temperatures, while the spike region increased due to the increase in ionic diffusion at higher temperatures.

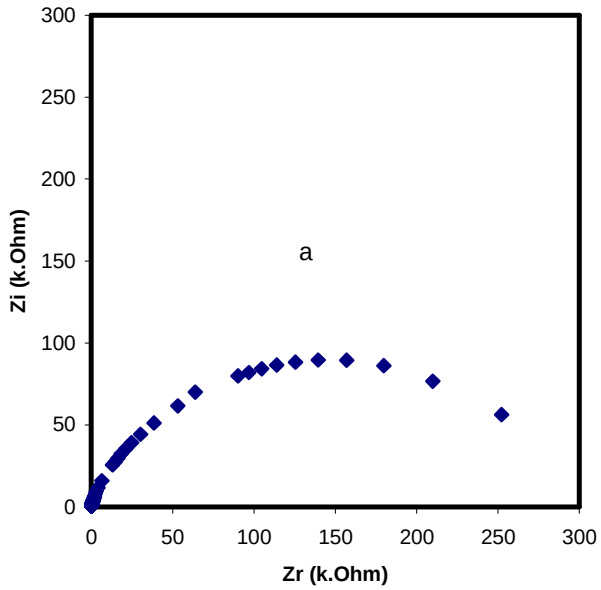

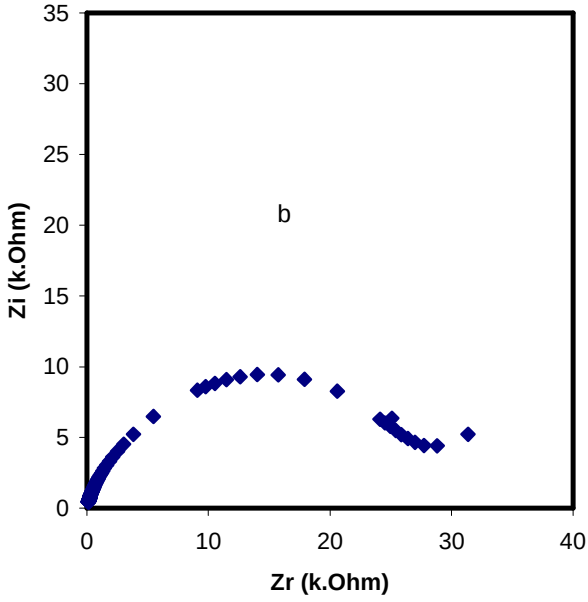

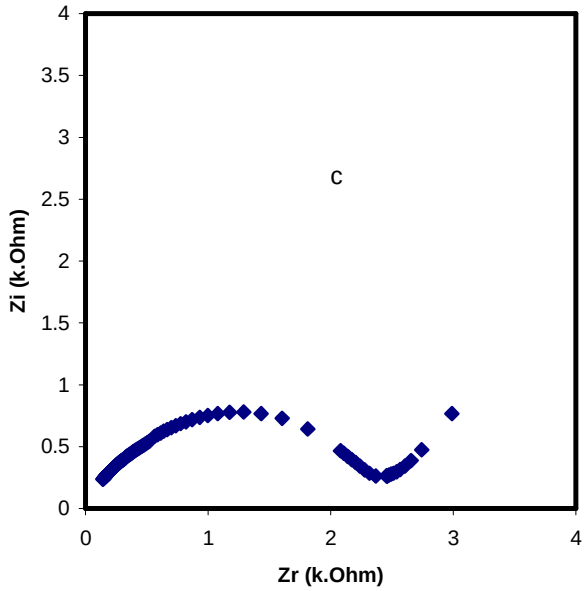
c
Zi (k.Ohm)
Zr (k.Ohm)
0
0.5
1
1.5
2
2.5
3
3.5
4

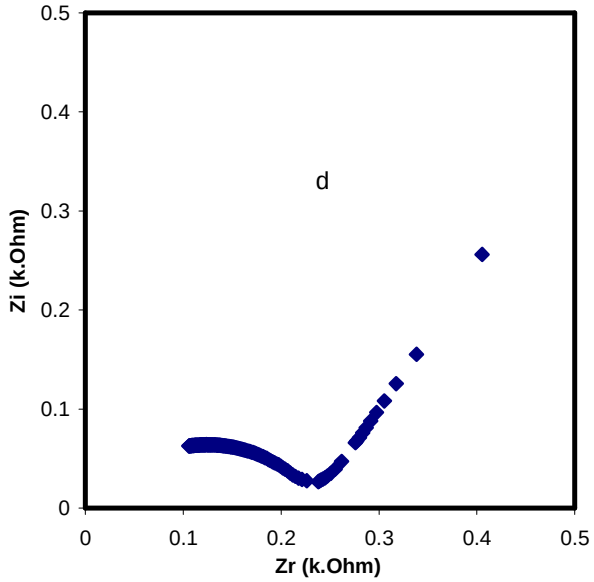
d
Zi (k.Ohm)
Zr (k.Ohm)
0
0.1
0.2
0.3
0.4
0.5

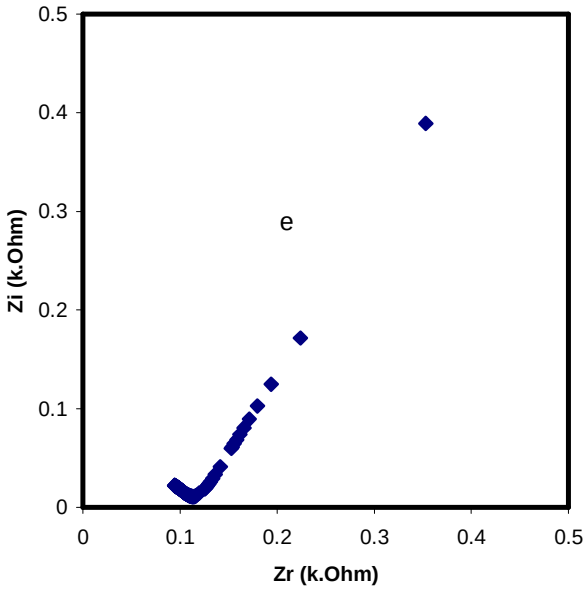

Figure 5.55 Impedance plot of chitosan:$LiCF_3SO_3$ (CSC6) at (a) 313 K, (b) 333 K, (c) 353 K, (d) 373 K, and (e) 393 K.

Figure 5.56 (a-f) shows AC conductivity as a function of frequency at different temperatures for chitosan-$LiCF_3SO_3$ (CSC6). The ac conductivity spectra from Fig 5.56 (a) to 5.56 (d) exhibit three distinct regions. The AC conductivity at low frequency region (I) which appeared as a spike can be ascribed to electrode polarization. This can be combined to the spike regions at different temperatures in impedance plots (Fig. 5.55). This behavior is also observed for the other two solid polymer electrolyte (CS:AgTf and CS:NaTf) systems. The plateau region in AC conductivity spectra corresponds to DC conductivity which shifts to high frequency with increasing temperature. In the high frequency region (III) the ac conductivity increases with increasing frequency and shows the power law dispersion. At higher temperatures the dispersion region disappeared as a result of electrode polarization dominance and a huge amount of charge accumulation. These results are strongly supported by impedance plots at high temperatures where only spikes are observed. From the overall results of these three systems we conclude that there is a strong

relationship between impedance plots and AC conductivity dispersion. To the best of our knowledge this is the first work which reveals electrode polarization effect on AC conductivity dispersion clearly.

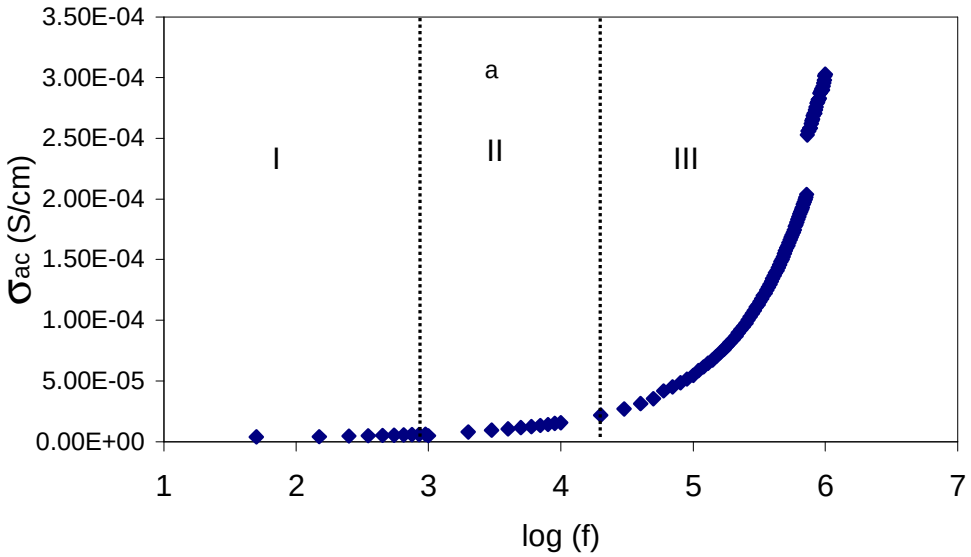

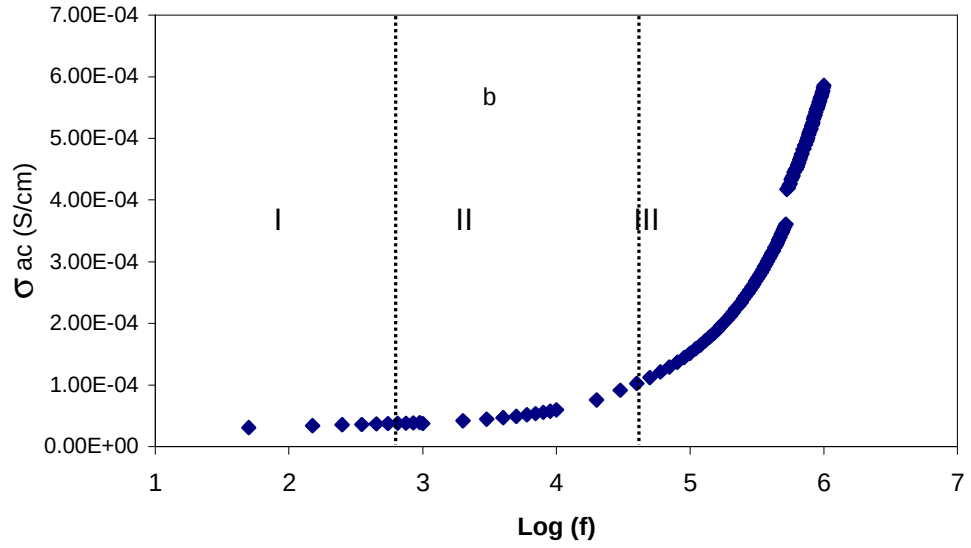

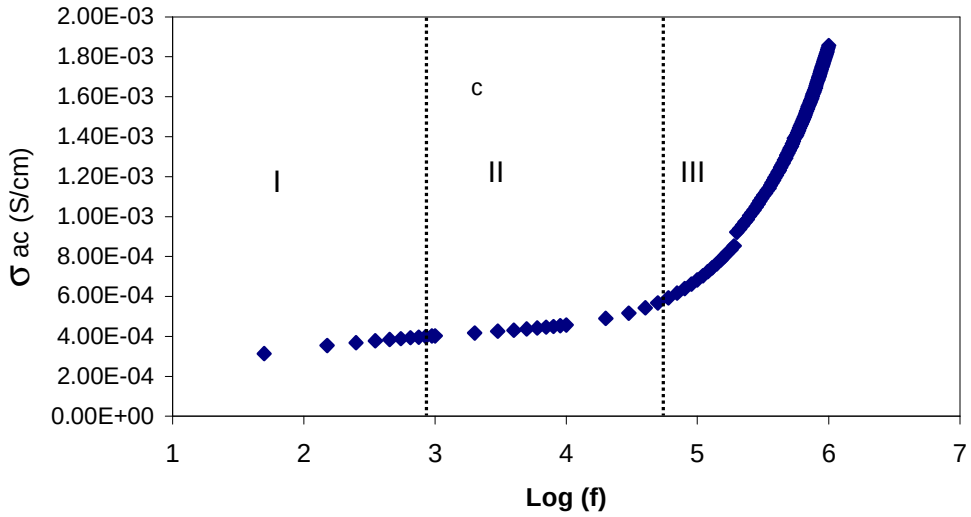
2.00E-03
1.80E-03
1.60E-03
1.40E-03
1.20E-03
1.00E-03
8.00E-04
6.00E-04
4.00E-04
2.00E-04
0.00E+00
σ ac (S/cm)
c
I
II
III
1
2
3
4
5
6
7
Log (f)

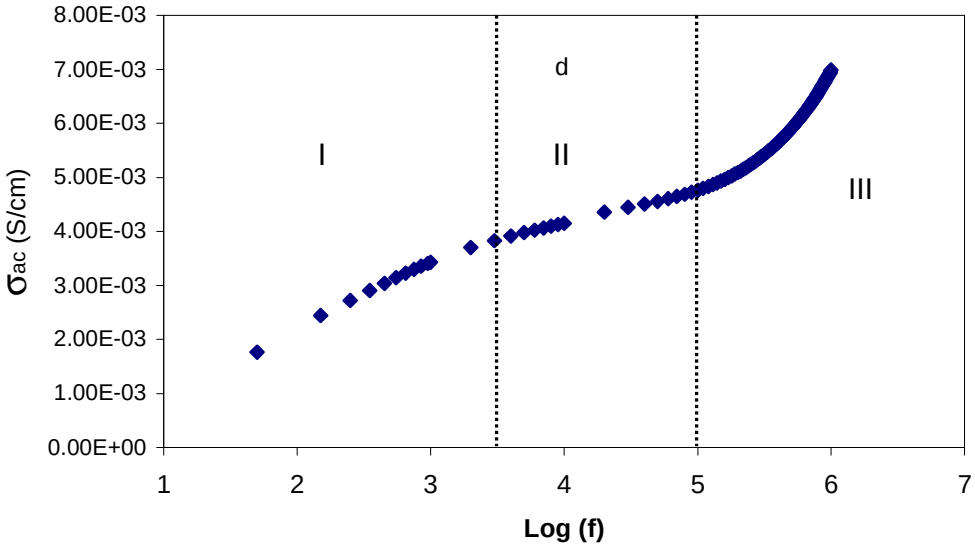
8.00E-03
7.00E-03
6.00E-03
5.00E-03
4.00E-03
3.00E-03
2.00E-03
1.00E-03
0.00E+00
σac (S/cm)
d
I
II
III
1
2
3
4
5
6
7
Log (f)

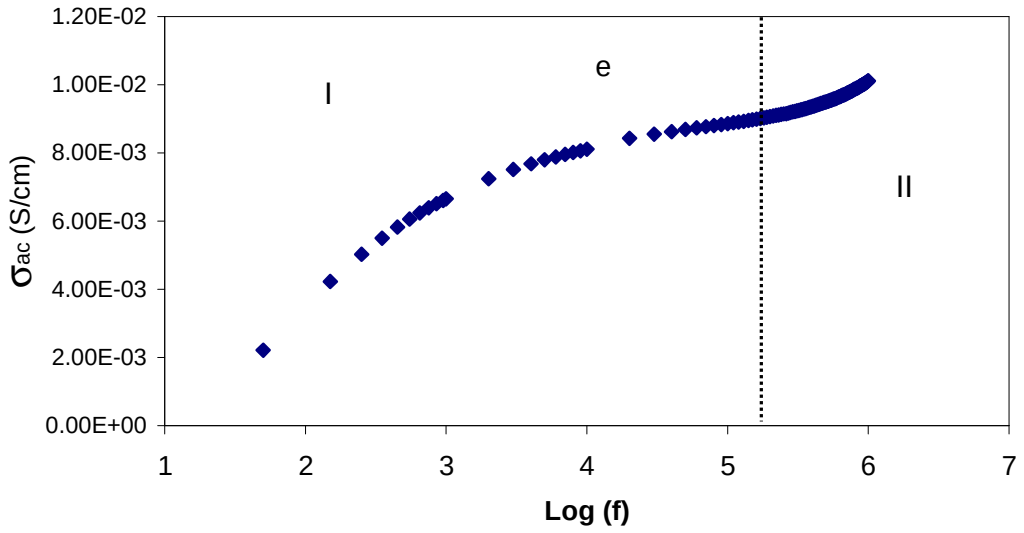

Figure 5.56 AC conductivity spectra of chitosan:$LiCF_3SO_3$ (CSC6) at (a) 313 K, (b) 333 K, (c) 353 K, (d) 373 K, and (e) 393 K.

To characterize the type of ion conduction in CS:LiTf solid polymer electrolyte the frequency exponent s is calculated from the slope of log (σ_{ac}) versus log (ω) at the dispersion region. As shown in Fig.5.57, the s value is temperature dependent; and it was observed that the s value decreased with increasing temperature to a minimum value and then increased slightly above 393 K. The behavior of frequency exponent (s) with temperature is very similar to that observed for the CS:NaTf (CSB6) system. Thus OLPT model is also applicable in CS:LiTf system.

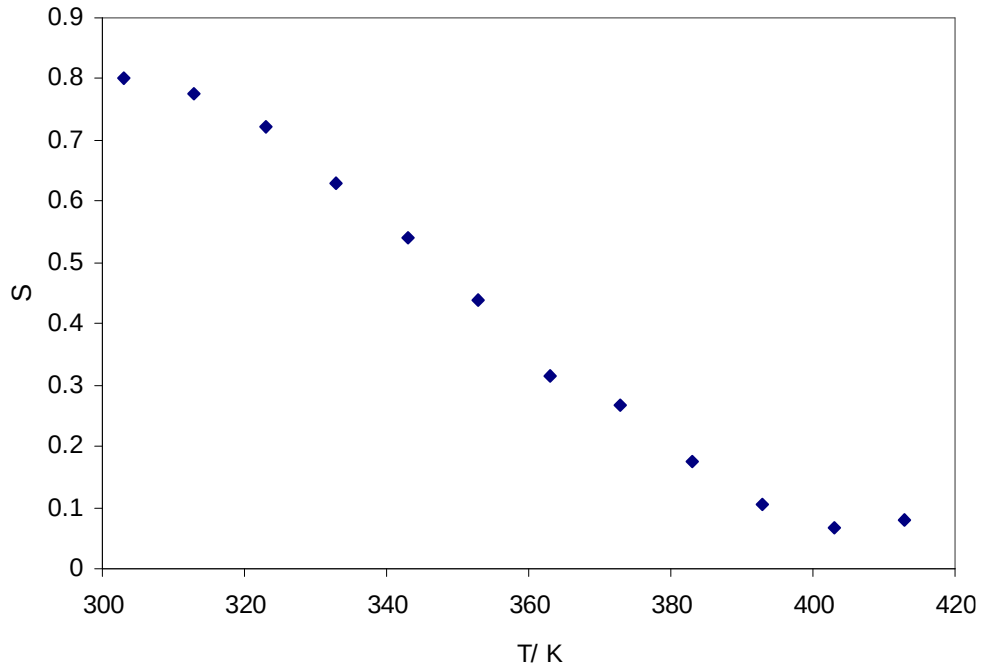

Figure 5.57 Temperature dependence of the frequency exponent s for CSC6 sample.

5.5 Summary

In this chapter some fundamental phenomena were demonstrated for the first time for solid polymer electrolytes. The basic principle between DC conductivity and dielectric constant were demonstrated successfully for three solid electrolyte systems. The DC conductivity and dielectric constant results indicate that the DC conductivity is not temperature dependent only but it also dependent on dielectric constant. The applicability of Arrhenius equation for these solid polymer electrolytes supports the motion of ion hopping in solid polymer electrolytes. The compensated Arrhenius behavior cannot be applicable for

chitosan based solid electrolytes. The random distribution of pre-exponential factor at different temperatures and dielectric constants for these SPEs (CS:AgTf, CS:NaTf and CS:LiTf) reveals the applicability of Arrhenius behavior. The relaxation processes in terms of Argant and Tan δ plots of theses solid polymer electrolytes supports the non-Debye ionic relaxation. Through the correlation between impedance and AC conductivity plots the electrode polarization effect on AC dispersion were demonstrated. The type of ion conduction for each system was specified from the Jonschers power law.